JOURNAL OF GEOPHYSICAL RESEARCH, VOL. 90, NO. B4, PAGES 3126–3144, MARCH 10, 1985

Spectral and Other Physicochemical Properties of Submicron Powders of Hematite (α-Fe_2O_3), Maghemite (γ-Fe_2O_3), Magnetite (Fe_3O_4), Goethite (α-FeOOH), and Lepidocrocite (γ-FeOOH)

RICHARD V. MORRIS,[1] HOWARD V. LAUER, JR.,[2] CHARLES A. LAWSON,[3] EVERETT K. GIBSON, JR.,[1] GEORG ANN NACE,[2] AND CHERI STEWART[2]

Spectral and other physicochemical properties were determined for a suite of submicron powders of hematite (α-Fe_2O_3), maghemite (γ-Fe_2O_3), magnetite (Fe_3O_4), goethite (α-FeOOH), and lepidocrocite (γ-FeOOH). The spectral reflectivity measurements were made between 0.35 and 2.20 μm over the temperature interval between about $-110°$ and 20°C. Other physicochemical properties determined were mean particle diameter, particle shape, chemical composition, crystallographic phase, magnetic properties, and Mössbauer properties. Only the magnetite powders have significant departures from the stoichiometric phase; they are actually cation-deficient magnetites having down to about 18.0 wt % FeO as compared with 31.0 wt % FeO for stoichiometric magnetite. A structured absorption edge due to crystal field transitions and extending from weak absorption in the near-IR to intense absorption in the near-UV is characteristic of the ferric oxides and oxyhydroxides and is responsible for their intense color. Particularly for hematite, the number and position of the spectral features are consistent with significant splitting of the degenerate cubic levels by noncubic components of the crystal field. The position of the crystal-field band at lowest energy, assigned to the envelope of the components of the split cubic $^4T_1$ level, is near 0.86, 0.91, 0.92, and 0.98 μm at room temperature for hematite, goethite, maghemite, and lepidocrocite, respectively. Comparison with Mössbauer data suggests covalent character increases sequentially through the aforementioned series. The positions of the spectra features are relatively independent of temperature down to about -110°C. The maximum shifts observed were on the order of about 0.02 μm shortward for the ferric oxyhydroxides. Variations in the magnitude of the reflectivity of the hematite powders as a function of mean particle diameter are consistent with scattering theory. The absorption strength of the crystal-field bands increases with increasing mean particle diameter over the range 0.1–0.8 μm; visually this corresponds to a change in color from orange to deep purple. The position of the split cubic $^4T_1$ band shifts longward by about 0.02 μm with decreasing mean particle diameter over the same range; this trend is consistent with wavelength-dependent scattering. The cation-deficient magnetite powders are very strong absorbers throughout the near-UV, visible and near-IR; their spectral properties are independent of temperature between about -110 and 20°C.

1. INTRODUCTION

It is well known from both theoretical considerations and laboratory experiments that variables including packing density, particle size and shape, and matrix composition influence the nature of the reflectance spectra of a particulate medium by changing its optical scattering characteristics. Another potentially important factor related to particle size is that the volumetric fraction of the near-surface volume of the individual particles becomes significant at small particle size. For example, the volumetric fraction of a 0.01 μm thick shell on the outside of a spherical particle is a relatively small 0.006 for a 10-μm-diameter particle but is a relatively large 0.88 for a 0.10-μm-diameter particle. The volumetric fraction of the near-surface volume is spectrally an important consideration when the spectral properties of the near-surface and interior volumes are different as can occur when the bulk composition is not in thermodynamic equilibrium with the surrounding medium. Similarly, the interface between the particles and surrounding medium prevents to some degree the development of the crystal structure or the magnetic ordering characteristic of bulk material in the near-surface volume.

This paper addresses the spectral properties (0.35–2.20 μm) of submicron powders of iron oxides and oxyhydroxides having the nominal mineralogy of hematite (α-Fe_2O_3), maghemite (γ-Fe_2O_3), magnetite (Fe_3O_4), goethite (α-FeOOH), and lepidocrocite (γ-FeOOH). A variety of other physicochemical data were also obtained for the powders in order to determine if deviations from stoichiometry occurred due to their small particle size as discussed above, to determine their state of chemical and phase purity, and to determine the physical characteristics of the individual powders. In addition to the spectral data, the physicochemical data we obtained included mean particle diameter, discrete particle shape, chemical composition, crystallographic phase, magnetic parameters, and Mössbauer parameters. The spectral properties of the iron oxides and oxyhydroxides are important not only for understanding the basic physics and chemistry of the compounds but also for applications such as the remote sensing of the earth and Mars.

2. SAMPLES

All of the iron oxides and oxyhydroxide powders used in this study are commercial products (Pfizer, Inc.). The general commercial availability of these materials is due to their industrial importance in such areas as pigments and in the manufacture of magnetic recording tape. In Table 1 we list the powders selected for this study, give their nominal composition and phase, and indicate their method of manufacture. We identify the powders by a four or five character name: the first two are letters for the mineral name of the nominal composition and phase (HM = hematite, etc.); the third character is always an S (for synthetic) for the powders used in this

[1]Experimental Planetology Branch, NASA Johnson Space Center, Houston, Texas.
[2]Lockheed, Houston, Texas.
[3]NASA Johnson Space Center, Houston, Texas.

Paper number 4B1323.
0148-0227/85/004B-1323$05.00

TABLE 1. List of Commercial Iron Oxide and Oxyhydroxide Powders Used in This Study

Powder	Nominal Compound	Pfizer Identification	Method of Manufacture
HMS1	α-Fe_2O_3	RO-3097	precipitation
HMS3	α-Fe_2O_3	R-1599	calcination of iron salts
HMS5	α-Fe_2O_3	R-8098	precipitation
HMS7	α-Fe_2O_3	RO-8097	calcination of iron salts
HMS9	α-Fe_2O_3	R-9998	calcination of iron salts
MHS3	γ-Fe_2O_3	MO-2230	α-FeOOH $\rightarrow$ α-Fe_2O_3 $\rightarrow$ Fe_3O_4 $\rightarrow$ γ-Fe_2O_3
MTS4	Fe_3O_4	BK-4799	precipitation
MTS5	Fe_3O_4	MO-4232	α-FeOOH $\rightarrow$ α-Fe_2O_3 $\rightarrow$ Fe_3O_4
MTS7	Fe_3O_4	CX-6147	α-FeOOH $\rightarrow$ α-Fe_2O_3 $\rightarrow$ Fe_3O_4
GTS2	α-FeOOH	YLO-1888B	precipitation
GTS3	α-FeOOH	YO-6087	precipitation
GTS5	α-FeOOH	YO-3587	precipitation
LPS2	γ-FeOOH	*	precipitation

*Not commercially available; special laboratory product.

study; and the last one or two characters are numbers for distinguishing powders having the same nominal composition and phase but different physical properties. An overview of the various manufacturing processes is given by *Hancock* [1975].

3. METHODS

3.1. *Particle Shape and Size*

The shape of the discrete particles and the mean particle size of the powders were determined from transmission electron photomicrographs. The transmission electron microscope employed was a JEOL 100-CX. The discrete particles were classified according to shape into the following five categories after *Hancock* [1975]: (1) spheroidal, (2) cubical, (3) nodular, (4) acicular, and (5) lamellar. The graphical procedure of *Folk and Ward* [1957] was used to calculate the mean particle size (M_z) and its standard deviation (σ) from particle volumes calculated from the dimensions of the particles. This mean particle size is thus referenced to mass and not number of particles.

3.2. *Composition*

The concentrations of nine major elements were obtained by X ray fluorescence analysis using the methods described by *Norrish and Chappell* [1967] and *Norrish and Hutton* [1969]. The concentration of ferrous iron was determined by chemical titration [*Maxwell*, 1968]. The elemental concentrations of C and S were determined using the procedure of *Gibson and Moore* [1973] and are reported as equivalent concentrations of CO_2 and SO_3, although we have no determination on the oxidation state of those two elements. The concentration of H_2O was determined coulimetrically with a DuPont 902H moisture evolution analyzer using the procedure outlined by *Morris and Lauer* [1981]. The parameter $(-)H_2O$ is the quantity of H_2O removed at room temperature in 30 min by the dry He stripping gas. The parameter $(+)H_2O$ is the quantity of H_2O subsequently evolved by heating to $\sim$650°C for 30 min. Both quantities are blank corrected. We take $(-)H_2O$ to represent the abundance of adsorbed H_2O and $(+)H_2O$ to represent the abundance of H_2O resulting from strongly bound H_2O and OH^- as in crystalline hydrates, hydroxides, and oxyhydroxides.

3.3. *Crystal Structure*

The crystalline phases present in the powders were identified from their X ray powder diffraction patterns obtained on a Picker powder diffractometer with Cu Kα radiation and a graphite-focussing monochromator. The compilation of X ray powder patterns for minerals by the Joint Committee on Powder Diffraction Standards (JCPDS) [*Joint Committee on Powder Diffraction Standards*, 1980] was used to identify crystalline phases.

3.4. *Thermogravimetric Analysis (TGA)*

The TGA data were acquired on a DuPont model 990 thermal analyzer. Either dry He or dry O_2 was used as the stripping gas. Usually a heating rate of $\sim$0.5°C/min was used.

3.5. *Magnetic Properties*

The hysteresis loops for diluted powders were obtained with a parallel-field vibration sample magnetometer (Princeton Applied Research Model 151). The saturation magnetization (J_s), saturation remanence (J_{rs}), and coercivity (H_c), were determined from it. The powders were diluted to $\sim$1% in Al_2O_3 (1 μm) by ultrasonic agitation in freon and subsequent vacuum drying at $\sim$30°C. Thermomagnetic data were acquired using a modified version of the standard high-temperature oven assembly for the magnetometer. The standard assembly was modified to permit a continuous flow of gas over the sample during heating. The gases used were either dry He or dry air. The sample containers were fabricated from boron nitride. Most thermomagnetic experiments were conducted in an applied magnetic field of 5.0 kOe. The heating rate was $\sim$10°C/min and the cooling rate was established by the thermal decay of the system after the power to the oven was shut off. Cooling to $\sim$100°C took about 4 hours, but the cooling rate is very nonlinear being rapid initially.

3.6. *Mössbauer Spectroscopy*

Mössbauer spectra were obtained at room temperature on an Elscint Mössbauer spectrometer using a 50 mCi Co^{57} (Rh) source and operating in the triangular mode with 1024 channels. The absorber thickness was about 10 mg Fe/cm^2, and all spectra had at least 10^6 counts/channel after folding about the mirror plane. The velocity scale was calibrated with a laser interferometer. The spectra were fit to Lorentzian lineshapes using a version of the program of *Stone et al.* [1971] furnished by M. D. Dyar (Massachusetts Institute of Technology) that we modified to use the data from the laser interferometer to calibrate the velocity scale. The Mössbauer parameters reported are the chemical isomer shift (IS) relative to the midpoint of the spectrum of metallic Fe foil, the quadrupole splitting (QS), and the internal field strength (H_{int}) for

TABLE 2. Summary of Selected Physical and Chemical Properties of Commercial Hematite (α-Fe_2O_3) Powders

Property*	HMS1	HMS7	HMS3	HMS5	HMS9
Shape	rhom.	rhom.	sph.	sph.	sph.
M_z	0.24	0.45	0.14	0.33	0.79
Range	0.20–0.29	0.35–0.59	0.11–0.19	0.22–0.50	0.67–1.01
J_s	0.33(6)	0.33(6)	0.22(6)	2.8(3)	6.5(4)
IS	0.38(1)	0.37(1)	0.37(1)	0.37(1)	0.37(1)
QS	−0.22(1)	−0.22(1)	−0.21(1)	−0.22(1)	−0.22(1)
H_{int}	512(2)	514(2)	512(2)	515(2)	514(2)
SiO_2	2.38	2.92	1.06	1.90	0.11
TiO_2	0.03	0.00	0.03	0.03	0.00
Al_2O_3	1.15	0.00	0.39	0.39	0.00
Fe_2O_3	93.14	95.51	97.40	95.86	97.75
FeO	0.35	0.18	0.19	0.79	1.68
MnO	0.00	0.08	0.00	0.25	0.35
MgO	0.17	0.45	0.14	0.34	0.00
CaO	0.17	0.05	0.06	0.14	0.00
K_2O	0.00	0.00	0.00	0.00	0.00
P_2O_5	0.00	0.02	0.00	0.06	0.02
SO_3	0.75	0.84	0.25	0.11	0.11
CO_2	0.52	0.08	0.04	0.09	0.03
$(+)H_2O$	1.91	1.02	0.27	0.20	0.08
$(-)H_2O$	0.46	0.11	0.29	0.10	0.08
Total	101.03	101.26	100.12	100.26	100.23

Errors are given in parenthesis and refer to the final digit.

*For particle shape, rhom. = rhombohedral, sph. = spherical, acic. = acicular. M_z = mean particle diameter in microns, and range = 1 standard deviation limit. J_s = saturation magnetization at 25°C in electromagnetic units per gram. Mössbauer parameters: IS = isomer shift relative to metallic Fe in millimeters per second; QS = quadrupole splitting in millimeters per second; H_{int} = internal field in kiloersteds. Compositions are in wt %.

Zeeman splitting. In the absence of Zeeman splitting, the value of QS was the magnitude of the doublet splitting. In the presence of Zeeman splitting, the value of QS was calculated from $1/2[(6-5)-(2-1)]$ where the numbers inside the brackets refer to the positions of the lines in the sextet numbered from lowest to highest velocity.

3.7. *Reflectance Spectroscopy*

Diffuse reflectivity spectra (0.35–2.2 μm) were acquired at room temperature in analog form on a Cary-14 spectrophotometer configured with a 9-inch-diameter integrating sphere. This configuration for a Cary-14 is described in detail by *Hedelman and Mitchell* [1968]. The interior coating of the integrating sphere and the reflectivity standard was Halon. The optical properties of this material are discussed by *Weidner and Hsia* [1981]. The sample containers for measurements at room temperature were filled to a depth of about 4 mm, and the entire instrument was purged with dry N_2 gas during measurements. The packing density of the powders in the sample holders unless otherwise noted was about 3.5 g/cm^3. The analog output of the Cary-14 was entered into a computer with a digitizer for data processing to remove baseline artifacts and to allow conversion to absolute reflectivity if required.

For measurements at subambient temperatures, a low-temperature device of our design was installed in the sample compartment of the Cary-14. It consisted of an aluminum metal sample cup mated to the top of a probe. The probe was cooled by circulating through it a fluid (either ethanol or N_2) whose temperature we can control; the accessible temperature range was between ambient and about −120°C. The sample cup was not in contact with the sample port of the integrating sphere to minimize both thermal losses from the sample cup and cooling of the sphere. The sample was located about 1.5 cm below the sample port. With this geometry, the reflectivity measurements are not truly total diffuse reflectivity because not all of the reflected radiation is collected by the integrating sphere. We used a sample thickness of about 0.5–1.0 mm for the subambient measurements (less than infinite in effective thickness) in order to minimize self insulation of the sample from the sample cup. Changes in the spectral properties of a particular sample were determined by comparison of ambient and subambient spectra acquired under the same conditions of geometry and sample thickness. We believe the subambient data are free of complicating effects of H_2O condensation, since we did not observe spectral features around 1.4 and 1.9 μm due to H_2O as the temperature was lowered.

4. HEMATITE POWDERS

4.1. *Material Properties*

The results for shape and dimensions of discrete particles, saturation magnetization (J_s), Mössbauer parameters, and composition are given in Table 2. The two hematite powders with rhombohedral particles (HMS1 and HMS7) were prepared by precipitation, and their mean particle diameters (M_z) are 0.24 and 0.45 μm. The three hematite powders with spheroidal particles (HMS3, HMS5, and HMS9) were prepared by calcination of iron salts, and their values of M_z are 0.14, 0.33, and 0.79 μm. The powders are well sorted (narrow particle size distribution) and the size distributions do not strongly overlap.

Chemically, the hematite powders are reasonably pure; the total iron content expressed as Fe_2O_3 ranges between 94 and 99 wt %. There are variable amounts of SiO_2 up to about 2.4 wt %; it is the major impurity in the hematites prepared by calcination of iron salts. For the hematites prepared by precipitation, SO_3 and $(+)H_2O$ are also present as significant impurities; they may be due to coprecipitation of minor phases or residues from the sulfate solutions. *Hancock* [1975] notes that goethite often coprecipitates during hematite synthesis, and this phase could be the origin of the $(+)H_2O$. Indeed, the TEM photomicrographs of HMS1 and HMS2 show some particles having the acicular shape characteristic of goethite. The chemical titrations indicate some ferrous iron is present.

The positions and relative intensities of the diffraction lines in the X ray powder patterns of the hematites conform to standard data [*JCPDS*, 1980]; no lines other than those attributable to the hematite structure were observed for any of the hematite powders. Minor phases, as could be present based on the chemical analyses, must then be present in quantities below the limit of detectibility or are amorphous to X rays. The diffraction lines were sharp (0.20°–0.30° 2θ halfwidth for the four most intense lines) indicating a high degree of crystallinity.

The Mössbauer spectra of all the hematite powders have the expected six-line Zeeman pattern as is shown in Figure 1 for HMS3 and HMS9. The values for the isomer shift (0.37–0.38 mm/s), quadrupole splitting (−0.21 to −0.22 mm/s), and internal field (512–515 kOe) are within error of the values reported in the literature [e.g., *Greenwood and Gibb*, 1971; *DeGrave et al.*, 1982].

Hematite is weakly magnetic with a saturation magnetization of approximately 0.5 emu/g [e.g., *Nagata*, 1961]. The measured values seem to depend on the nature of individual specimens. The values of J_s for HMS1, HMS3, and HMS7

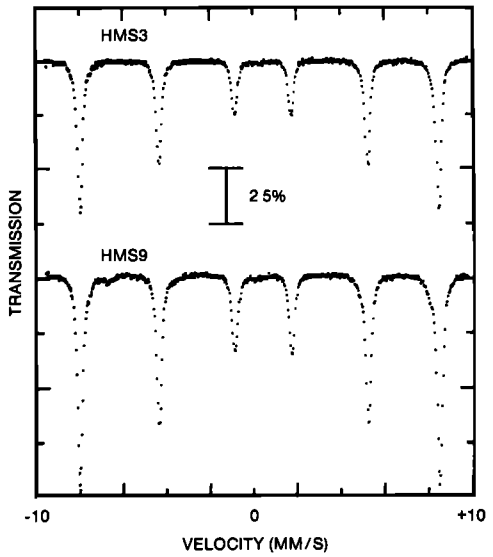

Fig. 1. Mössbauer spectra for hematite powders HMS3 and HMS9 at room temperature.

are consistent with hematite as the only phase since they fall in the range $0 < J_s \lesssim 0.5$. However, the 2.8 and 6.5 emu/g values of J_s for HMS5 and HMS9, respectively, are in excess of the values typically observed for hematite.

Thermomagnetic analyses through determination of Curie points or phase changes provide information about the composition of the magnetic phases. The thermomagnetic curve in air for HMS3 in Figure 2*a* shows only the Curie point characteristic of hematite at ~670°C [e.g., *Nagata*, 1961] so that, magnetically speaking, HMS3 is single phase hematite. For HMS1 and HMS7, an additional apparent Curie point is observed at about 350°C as can be seen in the thermomagnetic curve in air for HMS1 in Figure 2*b*. The transition at 350°C is probably a phase transition, since it is not observed to be reversible upon cooling. We will show later in this paper that

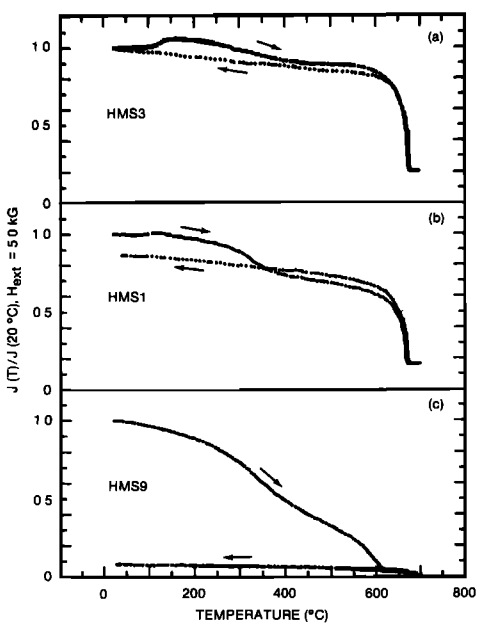

Fig. 2. Thermomagnetic curves for (*a*) HMS3, (*b*) HMS1, and (*c*) HMS9. All curves were obtained in air and an external magnetic field of 5.0 kG. Arrows denote heating and cooling curves.

maghemite inversion to hematite or magnetite oxidation to hematite can occur near 350°C. Based on the difference between the pre- and postheating values of J, the amount of either maghemite or magnetite necessary to account for the 350°C transition is ~0.3 wt % for maghemite (using $J_s = 74$ emu/g) or ~0.2 wt % for magnetite (using $J_s = 92$ emu/g).

The thermomagnetic curves for HMS5 and HMS9 show three apparent Curie points at about 400°, 625°, and 670°C as can be seen in the curve for HMS9 in Figure 2*c*. As before, the 670°C transition corresponds to the Curie temperature of hematite, and the irreversible nature of the curve indicates the other two transitions are probably phase transitions representing some combination of magnetite oxidation to hematite (or maghemite) and maghemite inversion to hematite. For the case of HMS5, about 4 wt % maghemite or about 3 wt % magnetite would account for the observed magnetic properties. For the case of HMS9, the required amounts are about 9 wt % maghemite or about 7 wt % magnetite. If the impurity phase is magnetite, then the chemical analyses for FeO should yield about 1 and 2 wt % for HMS5 and HMS9, respectively. This level of FeO content is in fact observed, but comparable levels are also observed for HMS1 and HMS7 which are not nearly so magnetic. Therefore, we feel that the strongly magnetic phase cannot be unambiguously identified with the available data.

In summary, the only powder which is single-phase hematite with respect to the X ray, Mössbauer, and magnetic data is HMS3. The other four powders are single-phase hematite with respect to the X ray and Mössbauer data but are not so when the magnetic data are taken into account. For HMS1 and HMS7, the magnetic properties can be explained by a small amount (0.2–0.3 wt %) of a strongly magnetic phase like maghemite or magnetite. For HMS5 and HMS9, the magnetic properties require 3–9 wt % of a strongly magnetic phase like maghemite or magnetite. Since we wish to obtain optical properties characteristic of hematite, we heated quantities of HMS5 and HMS9 in air at 640°C, a temperature which the thermomagnetic data showed will cause the magnetic impurities to convert to hematite. Similarly, we heated quantities of HMS1 and HMS7 at 350°C. An abridged set of material properties of the calcined powders are given in Table 3. Also given are corresponding data for two additional hematite powders (HMS14 and HMS15) formed by calcination of acicular goethite powders at 625°C. The identify of the phase was confirmed by X ray diffraction data, and the magnetic data did not indicate the presence of any strongly magnetic impurities. The properties of the precursor goethites are discussed later in this paper. The chemical data for all the precur-

TABLE 3. Summary of Selected Physical and Chemical Properties of Hematite Powders Derived by Calcination of Commercial Powders

Property*	HMS10	HMS11	HMS12	HMS13	HMS14	HMS15
Shape	rhom.	rhom.	sph.	sph.	acic.	acic.
M_z	0.24	0.45	0.33	0.79	0.05 × 0.40	0.1 × 0.7
J_s	0.25(6)	0.24(6)	0.28(6)	0.35(6)	0.02(3)	0.01(3)
$(+)H_2O$	0.25	0.12	0.05	0.06	0.23	0.09
$(-)H_2O$	0.21	0.13	0.07	0.09	0.28	0.13
Precursor	HMS1	HMS7	HMS5	HMS9	GTS2	GTS3
Calcination temperature	400	400	640	640	625	625

*See Table 1, except calcination temperature is in degrees Celsius.

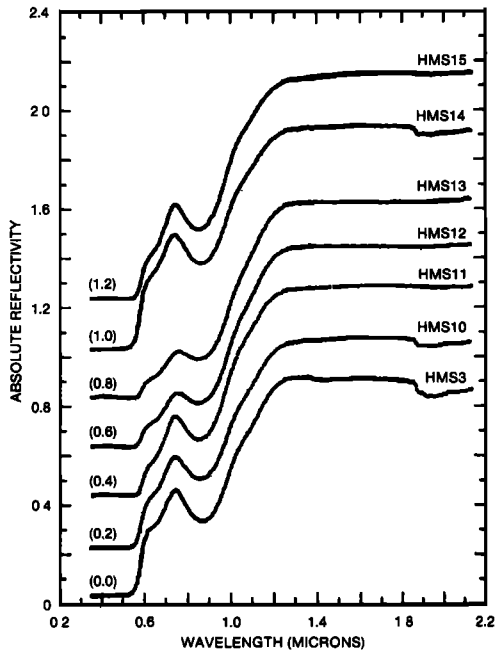

Fig. 3. Diffuse reflectivity spectra for seven hematite powders at room temperature. The spectra are stacked for clarity; the offsets are given to the left of each trace.

sors should be applicable to their derivatives by calcination after appropriate corrections for volatile loss. The particle shape and mean particle size of the derivatives were not measured but were taken to be equivalent to those for the corresponding precursor in accordance with *Hancock* [1975].

4.2. *Optical Properties: Room Temperature*

Spectra and band assignments. The diffuse reflectivity spectra for the eight hematite powders are given in Figure 3. For clarity the spectra are stacked; the offsets made along the reflectivity axis are given on the left side of the figure. The spectra are characterized by a nearly constant reflectivity in the near-IR, a knee near 1.03 μm, a band minimum near 0.86 μm, a local reflectivity maximum near 0.75 μm, a shoulder centered near 0.62 μm, and very low reflectivity shortward of about 0.55 μm. The measured positions of these features for each spectrum are compiled in Table 4.

The symmetry types for the ground (^6S) and first excited (^4G) states of d^5 ions such as ferric iron in crystal fields having

TABLE 4. Location of Spectral Features in Hematite Spectra at 25°C

Hematite	Absorption Edge[a]	Shoulder[a]	Local Reflectivity Maximum[b]	Band Minimum[b]	Knee[c]
HMS3	0.541	0.641	0.745	0.870	1.028
HMS10	0.542	0.641	0.745	0.859	1.028
HMS11	0.567	0.636	0.745	0.852	1.022
HMS12	0.558	0.632	0.755	0.847	1.031
HMS13	0.564	0.641	0.759	0.846	1.024
HMS14	0.535	0.639	0.744	0.861	1.018
HMS15	0.553	0.634	0.746	0.854	1.033

All wavelengths in microns.
[a]Error = ±0.010.
[b]Error = ±0.005.
[c]Error = ±0.03.

TABLE 5. States of Ferric Iron in Environments Having O_h (Cubic Class), D_3 (Trigonal Class), C_{4v} (Tetragonal Class), and C_{2v} (Orthorhomib Class) for the Ground (^6S) and First Excited (^4G) States of the Free Ion

Free Ion Term	Symmetry of Environment			
	O_h	D_3	C_{4v}	C_{2v}
^6S	$^6A_1$	$^6A_1$	$^6A_1$	$^6A_1$
^4G	$^4A_1$	$^4A_1$	$^4A_1$	$^4A_1$
	^4E	^4E	$^4A_1$	$^4A_1$
			$^4B_1$	$^4A_2$
	$^4T_1$	$^4A_2$	$^4A_2$	$^4A_2$
		^4E	^4E	$^4B_1$
				$^4B_2$
	$^4T_2$	$^4A_1$	$^4B_2$	$^4A_1$
		^4E	^4E	$^4B_1$
				$^4B_2$

cubic, trigonal, and orthorhombic symmetry are given in Table 5 (modified from *Cotton* [1963]). The ^6S state is unsplit and the ^4G state is split into four states in a cubic field, into six states in a trigonal field, and into nine states in an orthorhombic field. Energy-level diagrams have been calculated for cubic and trigonal symmetries, and specific examples are shown in Figure 4 (modified after *Konig and Kremer* [1977]). The parameters B and C are the Racah coefficients, and Dq is the cubic crystal-field parameter; $D\sigma$ and $D\tau$ are the trigonal crystal-field parameters. For cubic symmetry, the $^4A_1$ and ^4E levels always lie at the same energy so that there are three transitions from the ground state to the ^4G levels. For trigonal symmetry, there are six transitions.

Hematite has a trigonal crystal structure in which all the ferric ions are octahedrally coordinated to oxide ions [e.g., *Blake et al.*, 1966]. Although the crystal field is trigonal, its spectra are usually interpreted in terms of the energy-level diagram for cubic symmetry [e.g., *Huguenin*, 1977; *Marfunin*, 1979; *Hunt and Ashley*, 1979; *Strens and Wood*, 1979; *Singer*, 1982; *Sherman et al.*, 1982]. The band minimum and shoulder near 0.86 and 0.63 μm in our spectra are assigned to the $^6A_1 \rightarrow {}^4T_1$ and $^6A_1 \rightarrow {}^4T_2$ transitions, respectively. Assignments for the absorption edge near 0.55 μm in our spectra vary and include the approximate minimum of the $^6A_1 \rightarrow ({}^4E,$

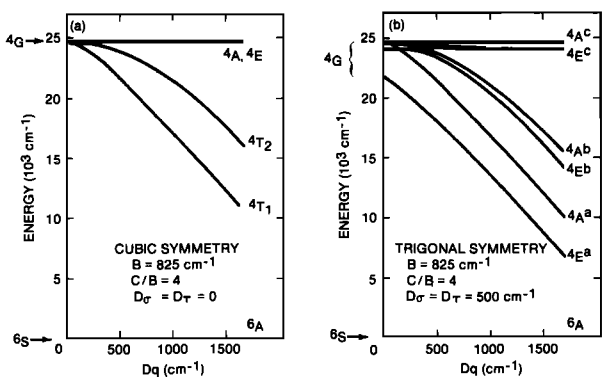

Fig. 4. Energy level diagram for ferric iron (high-spin d^5 configuration) in crystal fields having (*a*) cubic symmetry and (*b*) a trigonal symmetry (modified after *König and Kremer* [1977]). When the same crystal-field representation occurs more than once, it is labeled with a superscript (*a*, *b*, *c*, etc.) from lowest to highest energy.

$^4A_1$) band, the wing of an intense $^6A_1 \rightarrow (^4E, ^4A_1)$ absorption centered near 0.45 μm, and the wing of intense charge-transfer absorptions centered in the near-UV. Assigning the crystal-field bands in this way assumes the effect of the noncubic field actually present is at most to broaden the individual cubic bands. Incorrect assignments will result if separate bands occur as can be seen with reference to Figure 4.

An alternate assignment scheme based on the six bands possible for trigonal symmetry is to attribute the 0.86 μm minimum and 1.03 μm knee to an unresolved doublet resulting from splitting of the cubic $^4T_1$ level and to attribute the 0.63-μm shoulder and 0.55-μm edge to an unresolved doublet resulting from splitting of the cubic $^4T_2$ level. The bands due to the cubic (^4E, $^4A_1$) level presumably occur near 0.45 μm but are not observed in reflectivity spectra because the absorption is too intense in that spectral region. That there is in fact a crystal-field transition near 0.55 μ has been suggested by *Chen and Cahan* [1981] who studied hematite by elipsometric spectroscopy. We do not assign specific transitions for trigonal symmetry to the hematite spectral features because the order in which the trigonal energy levels occur for the quartet states is not independent of the crystal-field parameters as is the case for cubic symmetry [*Konig and Kremer*, 1977].

The above scheme is based in part on previous studies of other ferric iron compounds where deviations from cubic symmetry were used to interpret their spectral properties. *Wood and Remeika* [1967] attributed the shape of the lowest-energy band in their absorption spectrum of $Y_3Fe_5O_{12}$ (yttrium iron garnet) to an unresolved doublet resulting from noncubic symmetry for the octahedrally coordinated ferric iron. Particularly relevant are the spectral studies of ferric doped corundum [e.g., *Lehmann and Harder*, 1970; *Krebs and Maisch*, 1971] which like hematite has a trigonal crystal structure. The absorption spectra published by *Lehmann and Harder* [1970] have three bands at energies lower than that of a relatively sharp band at 0.45 μm which they reasonably assigned to the cubic $^6A_1 \rightarrow (^4E, ^4A_1)$ transition. Because only two bands at lower energies are possible for cubic symmetry, they suggested the bands at 0.57 and 0.70 μm are due to the split-components of the cubic $^4T_2$ level and the band at 1.06 μm is due to the cubic $^4T_1$ level.

Other explanations have been made for the 0.57 μm band observed by *Lehmann and Harder* [1970]. *Krebs and Maisch* [1971] argued it is due to a chromium impurity. We discount this possibility because it is not consistent with our unpublished spectra of chromium-doped corundum. *Lehmann and Harder* [1970] themselves noted it could be due to simultaneous excitation of two ferric ions to the $^4T_1$ level ($^6A_1 + {}^6A_1 \rightarrow {}^4T_1 + {}^4T_1$) because it occurs at approximately twice the energy of the $^4T_1$ band. For hematite, the same pair excitation would occur at approximately 0.43 μm based on the position of its $^4T_1$ band. Thus, if the 0.55-μm edge corresponds to the approximate position of a band minimum, it is more reasonably assigned to a split-component of the cubic $^4T_2$ level.

An alternative assignment for the band causing the 1.03-μm knee is a transition from $^6A_1$ to the level derived from the ^2I spectroscopic state which can occur near the $^6A_1 \rightarrow {}^4T_1$ transition in a crystal field having cubic symmetry [e.g., *Konig and Kremer*, 1977; *Marfunin*, 1979]. However, we view this as unlikely because the intensity of that transition should be relatively small because it is twice forbidden (spin forbidden and a two-electron transition). In contrast, transitions to the ^4G levels are only spin forbidden.

Marusak et al. [1980] published optical absorption spectra of thin films and crystal platelets of hematite. Their thin film spectra show two weak bands centered near 0.78 and 0.86 μm that are longward of a strong, broad, composite band whose edge is near 0.64 μm. The platelet spectra, which covered the range between 0.72 and 1.05 μm, show only a single band centered near 0.86 μm and flanked on both sides by shoulders of unknown origin. The absorption band centered near 0.86 μm in each case undoubtedly corresponds to the one also centered near 0.86 μm in the powder spectra. We do not see either evidence for their 0.78-μm band in our spectra or evidence for the parental band of our 1.03 μm knee in their spectra. The reason for these differences is not clear. *Marusak et al.* [1980] fit their data to the trigonal energy level diagrams of *Konig and Kremer* [1977], but we consider the assignments suspect until the differences noted above between the powder and thin-film spectra are understood and because for one of their bands the calculated value of 0.84 μm is substantially different from its measured position of 0.78 μm.

At present, the main factor favoring the assignment scheme based on significant splitting of the cubic energy levels over the cubic scheme is the evidence for a crystal-field transition occurring near 0.55 μm. This includes the study of *Chen and Cahan* [1981] and the preliminary studies of the spectral properties of the hematite-corundum series which indicate the 0.57-μm band in ferric-doped corundum corresponds to the 0.55-μm edge in hematite [*Morris and Lauer*, 1983]. However, all this needs confirmation, and it is clear that additional theoretical and experimental work are needed to fully understand the crystal-field spectra of hematite.

Whatever the origin of the 0.55-μm edge, at some wavelength below 0.55 μm the low reflectivity (0.02–0.04) from there through the near-UV is generally attributed to intense oxide $\rightarrow$ ferric charge-transfer transitions that occur in the near-UV for the FeO_6^{-9} complex ion [e.g., *Kahn et al.*, 1969]. *Tossel et al.* [1973] using SCF-$X\alpha$ methods calculated positions of the four lowest lying oxide $\rightarrow$ ferric charge-transfer transitions as 0.40, 0.34, 0.28 and 0.23 μm. The large absorption coefficient in this region, which is of the order of 10^5 cm^{-1} [*Marusak et al.*, 1980] is consistent with the fully allowed nature of these transitions. The relative strengths of the crystal-field absorptions and the wings of the charge-transfer absorptions at and below the 0.55-μm edge cannot be directly determined from reflectivity data because the very low reflectivity, which is predominently due to the regular part of the reflection, is a consequence of very strong absorption irrespective of its origin.

Effect of particle size and shape. In Figure 5 we plot the reflectivity at 0.60 μm as a function of the reflectivity ratio $R_{0.60}/R_{0.45}$ as a quantitative representation of brightness and visual color. The powders with the highest values of $R_{0.60}$ and $R_{0.60}/R_{0.45}$ are relatively bright and orange-red; the ones with the lowest values of those parameters are relatively dark and purple. We chose the above wavelengths because they are near or the same as those used in remote sensing applications [e.g., *Soderblom et al.*, 1978]. There are no apparent trends or clustering of data in Figure 5 which can be attributed to differences in the shapes of the discrete particles in the powders. We will next show that particle size is the variable which primarily determines the difference in the spectral properties among the hematite powders.

The procedure for calculating the mean grain size (M_z) for the powders having spheroidal and rhombohedral particles assumed the particles are perfect spheres. In order to have an

equivalent parameter for the powders with acicular particles, we calculated the diameter of a sphere whose volume is equal to the volume of the mean acicular particle. The variation of reflectivity at 1.60, 0.60, and 0.45 μm as a function of the equivalent spherical particle diameter D_s is shown in Figure 6. Those three wavelengths represent spectral regions in which the absorption by hematite is weak, intermediate, and strong, respectively. The reflectivities at 1.60 and 0.60 μm decreases with D_s, although at 0.60 μm the reflectivity is more nearly constant for $D_s \gtrsim 0.40$ μm. The reflectivity at 0.45 μm is nearly constant, but does tend to increase slightly with D_s. It is clear that the reflectivities at the three representative wavelengths vary in a regular way with particle size expressed as D_s, and in fact the observed trends are in accordance with previous studies relating reflectivity to particle size and absorption strength [e.g., *Wendlandt and Hecht*, 1966; *Vincent and Hunt*, 1968; *Kortum*, 1969]. When absorption is very strong, reflectivity tends to increase with particle size because the regular part of the reflection is predominant. When absorption is weak, the volume part of the reflection is predominant, and the direction of the variation of the reflectivity with particle size depends on the particle size relative to the wavelength of the incident radiation. For particle dimensions very much smaller than the wavelength, the scattering coefficient increases with increasing particle size corresponding to an increase in reflectivity. For particle dimensions greater than the wavelength, the scattering coefficient decreases with increasing particle size corresponding to a decrease in reflectivity. We observed the latter trend in our data at 1.60 μm even though the particle diameters are comparable to or less than 1.60 μm. That apparent inconsistency can be resolved if particle clumping occurs so that the effective diameter is larger than the actual diameter, a likely situation in our compacted powders.

The explanation for the 0.60-μm data is the same as that for the 1.60-μm data except that the nearly constant reflectivity at the larger values of D_s suggests that the absorption strength has increased to the point where the regular part of the reflection, which has the opposite dependence on particle size, has become important. An alternate explanation for the nonlinearity of the 0.60-μm data is that the relationship between reflectivity and particle size is nonlinear at low reflectivity. There is a basis in theory for the latter explanation because the volume part of the reflectivity is a nonlinear function of the scattering coefficient (and thus D_s), and deviations from approximate linearity are strong at low reflectivity [e.g., *Kortum*, 1969].

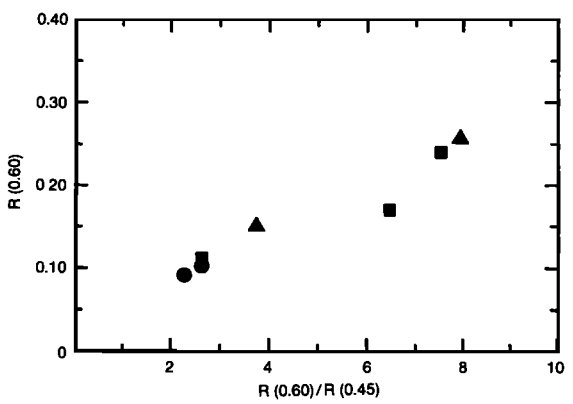

Fig. 5. Plot of the reflectivity at 0.60 μm against the ratio of the reflectivity at 0.06 μm to that at 0.45 μm for the hematite powders. The circles denote the powders having spheroidal discrete particles; squares, rhombohedral discrete particles; and triangles, acicular discrete particles.

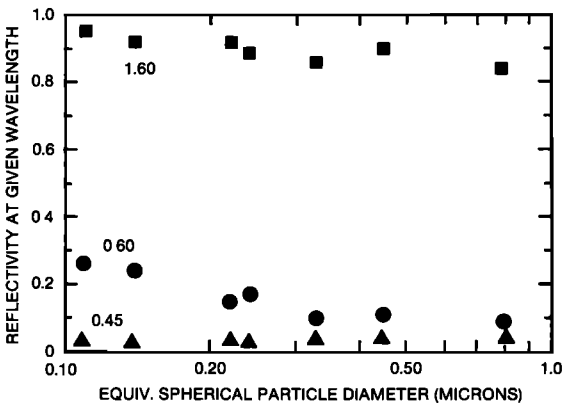

Fig. 6. Reflectivity at 0.45, 0.60, and 1.06 μm as a function of equivalent spherical particle diameter for the hematite powders.

In Figure 7 we plot the position of the band minimum occurring around 0.86 μm (i.e., the minimum of the envelope of the transitions to the split components of the cubic $^4T_1$ level) as a function of D_s. Although the range of the values of the minima is small ($\sim$0.03 μm) and comparable to the uncertainty, there does seem to be a longward shift in the position of the band minimum with decreasing particle size. Such an effect is a manifestation of wavelength-dependent scattering [e.g., *Wendlandt and Hecht*, 1966; *Kortum*, 1969; *Morris et al.*, 1982], and this process may be important here since $D_s \lesssim \lambda$ for our powders.

In summary, we find that the differences among the spectra of the hematite powders are reasonably attributed to differences in particle size. No effects of particle shape are apparent in our data, although on theoretical grounds they could be present.

Comparison of commercial and calcined commercial powders. We showed earlier that some of the commercial hematite powders are contaminated with small to moderate amounts of a strongly magnetic phase, presumably magnetite. As a typical example, we will compare the reflectivity spectrum of HMS9 with that of its derivative HMS13 by calcination to oxidize the magnetite. As shown by the spectra in Figure 8, the differences are greatest in the near-IR where the reflectivity of the contaminated hematite is lower than that of its calcined counterpart. This is consistent with the contami-

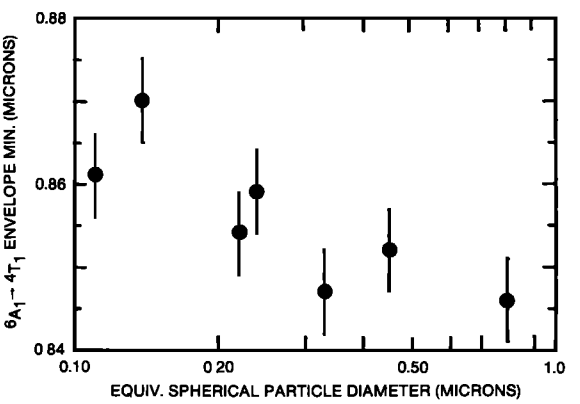

Fig. 7. Position of the $^6A_1 \rightarrow {}^4T_1$ envelope minimum as a function of the equivalent spherical particle diameter for hematite powders.

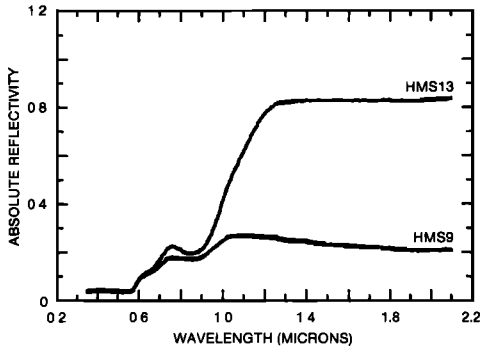

Fig. 8. Comparison of the diffuse reflectivity spectra of the magnetic (i.e., contaminated) hematite powder HMS9 to its derivative by calcination HMS13 to remove the strongly magnetic component. The spectra were acquired at room temperature.

nant being magnetite since it is optically opaque. Additionally, *Morris and Neely* [1982] published spectra of mechanical mixtures of hematite and magnetite which are very similar to those for the contaminated hematites.

4.3. *Optical Properties: Low Temperature*

The normalized reflectivity spectra for HMS3 and HMS13 at about +20° and −112°C are shown in Figure 9 over the spectral range 0.35–1.60 μm. Of our hematite powders, those two represent the extremes with respect to mean particle diameter; the temperature dependence of their spectral properties is typical for all of our hematite powders. As can be seen by comparing the room- and low-temperature spectra for each powder, lowering the temperature resulted in an apparent reduction in the width of the bands resulting in the observed general steepening of slopes and the small increase in optical contrast between the band minima and local reflectivity maxima. The reduction in width may be due to reduced thermal broadening. For HMS3, the reduction in band width was sufficient that the shoulder near 0.62 μm at 20°C resolved into a well-defined band minimum at 0.623 ± 0.005 μm by −112°C. In accordance with the discussion in the last section, this band would correspond to the transition from the $^6A_1$ ground state to the low energy component of the cubic $^4T_2$ level split by the trigonal crystal field. The positions of the absorption edge, the local reflectance maximum near 0.74 μm, and the band minimum near 0.87 μm for HMS3 and 0.85 μm for HMS13 are the same within experimental error at +20 and −112°C as can be seen in Figure 9. Spectra recorded at intermediate temperatures verify that relationship over the range +20° to −112°C. The knee at about 1.03 μm in the 20°C spectra is not apparent in the −112°C spectra. We infer that either the band causing this feature shifted to shorter wavelengths, or that its width became effectively narrower than that of the 0.85- to 0.87-μm band, or both.

Our results are consistent with those of *Marusak et al.* [1980] who found for the axial absorption spectra of hematite single crystals that the position of the absorption maximum near 0.86 μm was the same for spectra obtained at +7° and −36°C. In a spectrum obtained at −149°C, a temperature outside our range, they found the absorption maximum was shifted longward compared to the other two temperatures by 0.007 μm. In contrast, *Sherman et al.* [1982] found that the band minimum shifted shortward by about 0.04 μm upon cooling to −10°C for a natural sample of hematite. We would easily have detected a shift of this magnitude had it occurred for our hematite powders and are puzzled by the different results. Since we did not observe any shift over the common temperature interval for six well-documented hematite powders, there may be some unknown factor, perhaps chemical impurities, peculiar to the natural sample studied by *Sherman et al.* [1980] that causes the shift.

5. MAGHEMITE POWDERS

5.1. *Material Properties*

The results for shape and dimension of discrete particles, hysteresis parameters (J_s, J_{rs}, and H_c), Mössbauer parameters, and composition for the commercially prepared maghemite MHS3 are given in Table 6. The maghemite was prepared by the standard industrial procedure in which acicular goethite is subjected to the following reaction sequence: α-FeOOH → α-Fe_2O_3 → Fe_3O_4 → α-Fe_2O_3 [e.g., *Hancock*, 1975]. Throughout this process the acicular shape of the precursor is retained, and this shape for MHS3 was confirmed by our TEM analyses. Chemically, the major impurities are SiO_2 and SO_3. The chemical titrations indicate some ferrous iron is present.

The X ray powder pattern of MHS3 is consistent with the tetragonal form of maghemite [*JCPDS*, 1980]: In this form, the vacancies in the defect spinel structure are in the octahedral positions and are ordered so that $c/a = 3$ [e.g., *Murray*, 1979]. Maghemite is the only phase indicated, and the sharp diffraction lines (0.25°–0.30° 2θ half width for the four most intense lines) are consistent with a high degree of crystallinity.

Although maghemite is strongly magnetic, a range of values is reported in the literature for the saturation magnetization. *Johnson and Merrill* [1974] suggest that 73 ± 2 emu/g is a reasonable value for J_s at room temperature for maghemite obtained by low-temperature oxidation of magnetite. Our value of 74 ± 2 emu/g for MHS3 is essentially equivalent. The 0.46 value observed for the ratio J_{rs}/J_s is close to the theoreti-

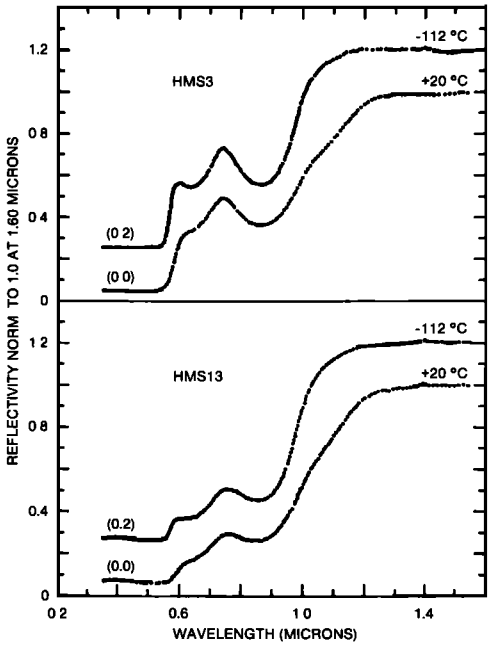

Fig. 9. Normalized reflectivity spectra for hematites HMS3 and HSM13 at about +20° and −112°C. The spectra were normalized to 1.0 at 1.60 μm. All of these spectra were obtained using the low-temperature sample probe and indicate reflectivities which are significant only in a relative sense (see "methods" section).

TABLE 6. Summary of Selected Physical and Chemical Properties of Commercial Maghemite (γ-Fe_2O_3) and Magnetite (Fe_3O_4) Powders

Property*	γ-Fe_2O_3, MHS3	Fe_3O_4 MTS4	Fe_3O_4 MTS5	Fe_3O_4 MTS7
Shape	acic.	cub.	acic.	acic.
M_z	0.05 × 0.3	0.50	0.09 × 0.6	0.07 × 0.3
Range	0.03 × 0.2 – 0.06 × 0.4	0.4–0.7	0.06 × 0.3 – 0.1 × 0.8	0.05 × 0.1 – 0.08 × 0.4
IS	0.32(1)	0.26(3); 0.70(3)†	0.26(3); 0.75(3)	0.26(3); 0.76(3)
QS	+0.01(1)	+0.06(3); −0.07(3)	+0.08(3); −0.08(2)	+0.07(3); −0.08(2)
H_{int}	499(6)	486(2); 462(2)	490(2); 468(2)	490(2); 470(2)
J_s	74(2)	81(2)	82(2)	84(2)
J_{rs}/J_s	0.46(2)	0.16(2)	0.43(2)	0.45(2)
H_c	378(25)	160(25)	410(25)	514(25)
SiO_2	2.63	0.47	0.00	2.56
TiO_2	0.00	0.01	0.10	0.00
Al_2O_3	0.00	0.34	0.15	0.06
Fe_2O_3	96.05	71.66	76.31	79.20
FeO	0.74	23.29	19.94	18.15
MnO	0.09	0.72	0.20	0.12
MgO	0.33	0.42	0.18	0.31
CaO	0.02	0.52	0.09	0.05
K_2O	0.00	0.00	0.00	0.00
P_2O_5	0.00	0.03	0.00	0.02
SO_3	1.30	0.13	1.46	0.56
CO_2	0.03	0.33	0.09	0.02
(+)H_2O	0.50	0.40	0.28	0.27
(−)H_2O	0.53	0.16	0.34	0.27
Total	102.22	98.44	99.14	101.59

Errors are given in parenthesis and refer to the final digit.

*See Table 1. J_{rs}/J_s = ratio of saturation remanance to saturation magnetization at 25°C. H_c = coercivity at 25°C in oersteds.

†Tetrahedral site; octahedral site.

cal value of 0.5 expected for randomly oriented, noninteracting, single-domain grains having uniaxial anisotropy [*Stoner and Wohlfarth*, 1948]. This is consistent with the small size and acicular shape of the discrete particles as determined by our TEM work. The thermomagnetic curve for MHS3 is shown in Figure 10. Only one transition at ~650°C is observed. Because of the irreversible nature of the curve, this transition is probably the phase transition corresponding to γ-$Fe_2O_3 \rightarrow \alpha$-$Fe_2O_3$ rather than a Curie point. *Nagata* [1961] suggests 675°C may correspond to the Curie point for maghemite.

The Mössbauer spectrum of MHS3 in Figure 11 shows apparently only a single sextet having an isomer shift of 0.32 mm/s, an internal field of 499 kOe, and a quadrupole splitting

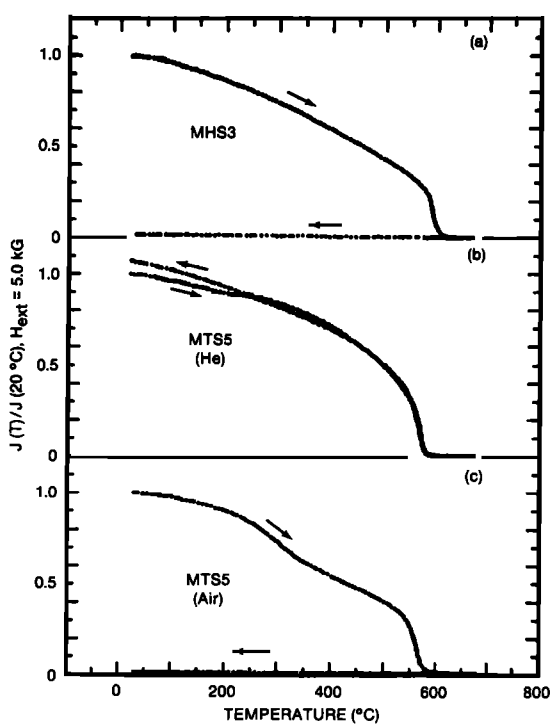

Fig. 10. Thermomagnetic curves in an external magnetic field of 5.0 kG for (*a*) maghemite MHS3 in an air atmosphere, (*b*) magnetite MTS5 in a He atmosphere, and (*c*) magnetite MTS5 in an air atmosphere.

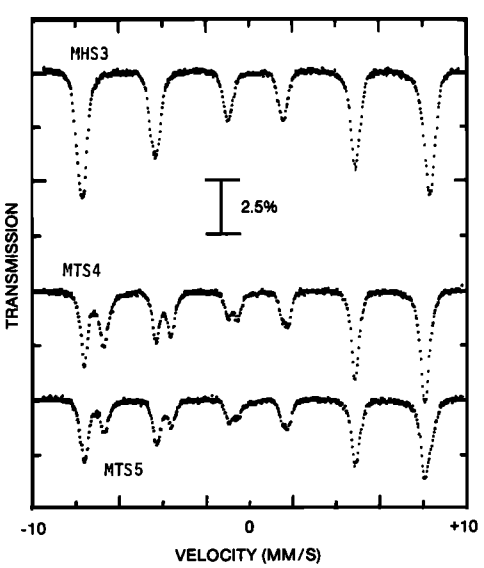

Fig. 11. Mössbauer spectra for maghemite powder MHS3 and cation-deficient magnetite powders MTS4 and MTS5 at room temperature.

TABLE 7. Summary of Chemical and Physical Properties of Maghemite Powders Derived by Calcination of Commerical Powders

Property*	MHS4	MHS5	MHS6
Shape	acic.	acic.	acic.
M_z	0.05 × 0.3	0.09 × 0.6	0.07 × 0.3
IS	0.32(1)	0.32(1)	0.32(1)
QS	0.00(1)	+0.01(1)	−0.01(1)
H_{int}	498(6)	500(6)	499(6)
J_s	72(2)	74(2)	76(2)
J_{rs}/J_s	0.44(2)	0.44(2)	0.42(2)
H_c	345(25)	333(25)	347(25)
Precursor	MHS3	MTS5	MTS7
Calcination temperature	350	325	325

*See Tables 1 and 2.

equal to zero within experimental error. Based on the work of *Armstrong et al.* [1966], this spectrum is most likely instead an unresolved superposition of two sextets, one each from the tetrahedrally and octahedrally coordinated ferric ions. They showed that application of an external magnetic field resulted in partial resolution of the two sextets and determined that the internal fields and isomer shifts for the tetrahedral and octahedral ferric ions are 488 and 499 kOe and 0.27 and 0.41 mm/s, respectively, in a zero applied external field. Our Mössbauer parameters agree most closely with those for the octahedral sextet presumably because it is more intense [*Armstrong et al.*, 1966].

In summary, MHS3 is single-phase maghemite with respect to the X ray, magnetic, and Mössbauer data. The FeO determination, however, indicates a small amount of magnetite or some other ferrous phase may be present. If the impurity is magnetite, then the equivalent of ~2 wt % either as a separate phase or a solid solution with maghemite is required to give the observed FeO content. In order to lower the FeO content of MHS3 and to provide additional powders of maghemite with somewhat different grain sizes, we calcined MHS3 and acicular magnetites MTS5 and MTS7 in air at ~325°C for ~300 hours. The properties of the magnetites are discussed in the next section, and it is also shown there that 325°C is sufficient to oxidize magnetite. An abridged set of the material properties of the derived powders are given in Table 7. As with the hematites in the last section, the grain size and shape data were taken to be the same as those for the precursors. The rest of the data were measured on the derived powders. The hysteresis and Mössbauer parameters for MHS4, MHS5 and MHS6 are within experimental error of the corresponding values for MHS3. The X ray diffraction data for MHS4, MHS5, and MHS6 are consistent with the powders being single-phase maghemite (tetragonal form); their thermomagnetic curves are essentially identical to the one for MHS3 in Figure 7 and thus also indicate single-phase maghemite.

We also attempted to make maghemite by dehydration of the acicular lepidocrocite powder (γ-FeOOH) discussed in a later section. The highest value of J_s we were able to obtain for lepidocrocite (LPS2) dehydrated at various temperatures for various times was ~53 emu/g, which is significantly lower than that for the maghemites previously discussed. The thermomagnetic data shows the transition to hematite occurs near 350°C, which is about 300°C lower than the temperature for the same transition for MHS3. The X ray diffraction data had only a few broad peaks at high angles so that these dehydrated lepidocrocites are nearly amorphous to X rays. Since we are not able to positively identify these dehydrated lepidocrocites as single-phase maghemite of some form by our criteria, we will not consider them further.

5.2. *Optical Properties: Room Temperature*

Spectra and band assignments. The diffuse reflectivity spectra for maghemites MHS4, MHS5, and MHS6 are given in Figure 12. The spectra are characterized by a nearly constant reflectivity in the near-IR, a knee near 1.15 μm, a band minimum near 0.92 μm, a local reflectivity maximum near 0.78 μm, a feature centered near 0.63 μm which ranges between a strong shoulder and a plateau, and very low reflectivity shortward of about 0.49 μm. The measured positions of those features are compiled in Table 8. In addition to the aforementioned spectral features there is a hint of a shoulder near the absorption edge at about 0.49 μm.

Maghemite has a spinellike crystal structure that is cation deficient. The actual structure depends on the distribution of the cation vacancies among the tetrahedral and octahedral sites which in turn seems to depend on the method of synthesis [e.g., *Lindsley*, 1976]. As discussed previously, the presence of tetragonal diffraction peaks in the X ray powder diffraction patterns of our maghemites indicate that the tetragonal maghemite phase is present; that structure seems to be the one favored by the oxidation of acicular magnetite [e.g., *Bernal et al.*, 1959]. In the tetrahedral form of maghemite, all cation vacancies occur in the octahedral positions. Therefore, whether or not other forms of maghemite are present, our maghemite powders would contain both tetrahedrally and octahedrally coordinated ferric iron, and both coordinations can be expected to contribute to the reflectance spectrum.

The cubic energy level diagram in Figure 4*a* is appropriate for both octahedrally and tetrahedrally coordinated ferric iron, but the magnitudes of the cubic crystal-field strengths are different and are related theoretically by $Dq_{tetra} = -(4/9)Dq_{oct}$ for equivalent ferric-oxide bond lengths [e.g., *Low*, 1960]. Therefore, the band minimum near 0.92 μm and knee near 1.15 μm would correspond to transitions from the $^6A_1$ ground state to the split-components of the cubic $^4T_1$ level for octahedrally coordinated ferric iron. The plateau or strong shoulder centered near 0.62 μm could be assigned to transitions from $^6A_1$ to either a split component of the cubic $^4T_2$ level of

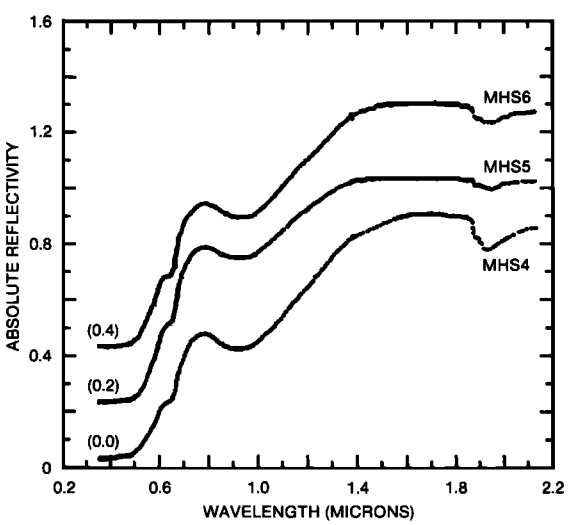

Fig. 12. Diffuse reflectivity spectra for maghemite powders at room temperature.

octahedrally coordinated ferric iron or a split-component of the cubic $^4T_1$ level of tetrahedrally coordinated ferric iron, or perhaps both. The region of strong absorption shortward of the absorption edge near 0.49 μm is most reasonably attributed to the intense oxide→ferric charge-transfer transitions together with superimposed weaker bands. We discussed previously for hematite that the charge-transfer transitions for octahedrally coordinated ferric iron (FeO_6^{-9} complex ion) occur in that region. We are not aware of any theoretical calculations, like those of *Tossell et al.* [1973] for the FeO_6^{-9} complex ion, for the transition energies of the charge-transfer transitions of tetrahedrally coordinated ferric iron (FeO_4^{-5} complex ion).

Sherman et al. [1982] have recently discussed the spectral properties of maghemite in connection with its possible occurrence on the surface of Mars. While the samples upon which their discussion was based are suitable for use as possible Martian spectral analogues, they are not particularly well-suited for the purpose of the spectral characterization of maghemite. All but one sample apparently contained appreciable ferrous iron; if so, they are not, chemically speaking, maghemite. The remaining sample, produced by the thermal dehydration of lepidocrocite, was very poorly crystallized. As discussed earlier, we likewise obtained poorly crystallized maghemite by the same method, and, in fact, its reflectivity spectrum is quite similar to the spectrum (M-5) published by *Sherman et al.* [1982]. The generally lower degree of spectral contrast and structure of the spectra of the poorly crystallized maghemites as compared to the spectra of the well-crystallized maghemites in Figure 12 is probably a consequence of the smearing of spectral features associated with decreased crystalline order. For example, the plateau centered near 0.63 μm in the crystalline maghemite spectra is relatively hardly distinguishable in the spectra of the dehydrated lepidocrocites.

Effect of particle size and shape. We studied only three maghemite powders and, because they all had the same acicular shape and their mean particle diameters span a narrow range, a detailed analysis of the effect of particle size and shape is not possible. It is worthwhile to note, however, that reflectivity in the visible and near-IR up to ~1.1 μm does seem to increase with D_s. For example, the reflectivity at 0.60 μm varies from ~0.21 for MHS4 ($D_s = 0.10$ μm) to 0.26 for MHS5 ($D_s = 0.19$ μm). The direction of this variation is opposite to the one observed at 0.60 μm for the hematite powders (see Figure 6) and the one expected on the basis of absorption strength as discussed in connection with the hematite spectra. If the trend for the maghemite data is real, we do not have a consistent explanation. Perhaps the maghemite trend is a manifestation not evident in our other data of different proportions of maghemites having different structural modifications, e.g., tetragonal versus cubic.

TABLE 8. Location of Spectral Features in Maghemite Spectra at 25°C

Maghemite	Absorption Edge[a]	Plateau Center[a]	Local Reflectivity Maximum[a]	Band Minimum[a]	Knee[b]
MHS4	0.488	0.627	0.776	0.919	1.158
MHS5	0.492	0.634	0.783	0.926	1.140
MTS6	0.488	0.630	0.781	0.937	1.151

All wavelengths in microns.
[a]Error = ±0.010.
[b]Error = ±0.030.

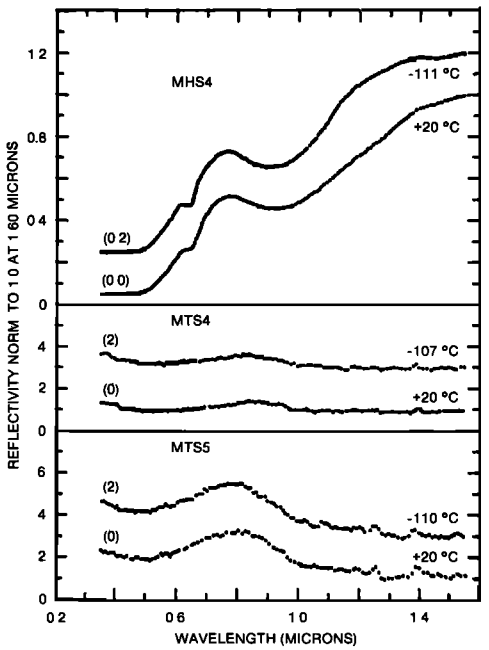

Fig. 13. Normalized reflectivity spectra for maghemite powder MHS4 and cation-deficient magnetite powders MTS4 and MTS5 at about +20° and −110°C. See caption of Figure 9.

5.3. *Optical Properties: Low Temperature*

The changes in the spectra of MHS4 with temperature are representative for the maghemite powders, and its normalized reflectance spectra at +20° and −111°C are shown in Figure 13. As was the case for the temperature dependence of the hematite spectra, a general steepening of all the slopes occurred as the temperature was reduced. This resulted in a plateau centered near 0.63 μm by −111°C instead of the strong shoulder observed there at 20°C. The band minimum near 0.91 μm is also more asymmetric at −110°C providing additional evidence this feature is a composite band. Within about 0.01 μm, the positions of all the spectral features at room temperature tabulated in Table 8 are the same at −111°C and at intermediate temperatures.

6. MAGNETITE POWDERS

6.1. *Material Properties*

The chemical and physical properties of the commercially prepared magnetite powders are given in Table 6. The magnetite powder having cubical particles (MTS4) was prepared by a precipitation technique. The other two magnetite powders (MTS5 and MTS7) have acicular particles and were prepared from acicular goethite by the following reaction sequence: α-FeOOH→α-Fe_2O_3→Fe_3O_4. The powders are reasonably pure with SiO_2 and SO_3 being the major chemical impurities.

The X ray powder diffraction patterns of MTS4, MTS5, and MTS7 are consistent with single-phase magnetite [*JCPDS*, 1980]. The diffraction lines are sharp (0.20°–0.30° 2θ half width for the four most intense lines) indicating a high degree of crystallinity. The FeO data show and the J_s and Mössbauer data confirm that all the magnetite powders are actually cation-deficient magnetites, i.e., deficient in ferrous iron compared to stoichiometric magnetite. The powders have 18 to 23 wt % FeO as compared to 31 wt % for stoichiometric mag-

netite. The values of J_s range between 81 and 84 emu/g compared to 92 emu/g for stoichiometric magnetite [e.g., *Nagata*, 1961]. The Mössbauer spectra for MTS4 and MTS5 are shown in Figure 11. The sextet having the lower value of H_{int} is due to the ferrous and ferric ions on the octahedral sites, and the one having the higher value is due to the ferric ions on the tetrahedral sites [e.g., *Greenwood and Gibb*, 1971]. For our powders, the absorption intensity of the former sextet is less than that for the latter while for stoichiometric magnetite the opposite is true [e.g., *Greenwood and Gibb*, 1971]. Note that the intensity of the ferrous-ferric sextet for MTS5 is less than that for MTS4 in agreement with their relative FeO contents. It is possible that the high degree of cation deficiency is due to the combination of the thermodynamic susceptibility of magnetite to oxidation in air at ambient conditions [e.g., *Gooding*, 1979] and the high surface to volume ratio of the powders. The absence of lines due to hematite and maghemite in the X ray diffraction data indicates the powders are cation deficient because the constituent particles are solid solutions (either homogeneous or heterogeneous) of Fe_2O_3 and Fe_3O_4 rather than macroscopic assemblages of Fe_2O_3 and Fe_3O_4 as could occur with a Fe_2O_3 composition shell surrounding a Fe_3O_4 composition core. The interpretation of *Daniels and Rosencwaig* [1969] for the Mössbauer spectra of cation deficient magnetites is also consistent with this view, although it would probably be difficult to distinguish between the maghemite sextet and the tetrahedral sextet of magnetite. Cation deficiency is apparently a commonly observed phenomenon in fine powders of magnetite [e.g., *Dunlop*, 1973; *Morris and Lauer*, 1980].

The thermomagnetic and thermogravimetric data give additional evidence for the view that the cation-deficient magnetite powders are Fe_2O_3-Fe_3O_4 solid solutions. The thermomagnetic curves recorded for both air and He atmospheres for MTS5 are typical and are given in Figure 10. The transition at $\sim 575°$ corresponds to the literature value for the Curie point of magnetite [e.g., *Bozorth*, 1951; *Nagata*, 1961]. Two factors lead us to conclude the irreversible transition near 450°C for the sample heated in air is due to oxidation of some of the cation-deficient magnetite to the weakly magnetic hematite as opposed to inversion of maghemite to hematite. First, under the more reducing conditions of the He atmosphere, the transition near 450°C is not observed. And second, thermogravimetric data (not given) obtained in air and in He atmospheres showed in the former case a gain in sample weight around 450°C, for which a reasonable interpretation is the uptake of oxygen during oxidation, and in the latter case no observable gain in weight.

In summary, the nominal magnetite powders are actually cation-deficient magnetites. While we would prefer to perform our spectral measurements on fine powders having the stoichiometric amount of FeO (31.0 wt %), we currently have no way to remove the cation deficiency from the powders by using reducing conditions without exposing them to oxidizing conditions prior to or during the spectral measurements. Consequently, the spectral properties we will discuss next pertain to cation-deficient magnetite powders and represent those of magnetite to the extent that their respective spectral properties are equivalent. This is not a limitation in the sense severe cation deficiency is the usual situation for fine magnetite powders exposed to oxidizing environments.

6.2. *Optical Properties: Room Temperature*

Spectra and band assignments. The diffuse reflectivity spectra of cation-deficient magnetites MTS4, MTS5, and MTS7 are given in Figure 14; for clarity the spectra are stacked. As is clearly evident, the diffuse reflectivity of the cation-deficient magnetites is very low throughout our spectral range. The maximum in reflectivity, which is ~ 0.04 for MTS4 and ~ 0.05 for MTS5 and MTS7, occurs at a weak reflectivity maximum centered in the region ~ 0.73–0.81 μm. The reflectivity in the near-IR longward of the maximum is nearly constant; the reflectivity for both MTS5 and MTS7 in this region is ~ 0.015 and that for MTS4 ~ 0.025.

Magnetite has an inverse cubic spinel crystal structure so that the ferrous ions occupy octahedral sites and the ferric ions occupy both tetrahedral and octahedral sites. Antiferromagnetic coupling of the magnetic moments of iron ions on the tetrahedral and the octahedral sites and the fact that there are more ions on the octahedral sites result in the ferrimagnetism of magnetite. At temperatures higher than $\sim$ 120°K (the Verwey transition; *Verwey and Haayman* [1941]), the octahedrally-coordinated ferrous and ferric ions are equivalent due to electron delocalization as is evident in Mössbauer spectra which show only two sets of lines, one from the tetrahedral sites and one from the octahedral sites [e.g., *Daniels and Rosencwaig*, 1969]. Upon cooling through the Verwey transition, the ferrous and ferric ions on the octahedral sites become distinguishable and apparently a change in crystal structure also occurs [e.g., *Goodenough*, 1980]. Of significance for this study is that *Daniels and Rosencwaig* [1969] also showed that the above considerations also are valid for cation-deficient magnetite, although the temperature of the Verwey transition is lower or not observed depending on the magnitude of the deficiency.

The lack of spectral structure and the very low diffuse reflectivity of our cation-deficient magnetites means the absorption coefficient is very large throughout the spectral range we studied. This is in fact the case, at least for magnetite. *Schlegel et al.* [1979] have determined and discussed the optical properties of naturally-grown single crystals of magnetite over the spectral range ~ 0.1–25 μm. Their results show that the absorption coefficient at room temperature is in excess of 60,000 cm^{-1} over the spectral range of our study. By comparison, the absorption coefficient for hematite at room temperature is approximately 1500 cm^{-1} at the center of the band near 0.86 μm [*Marusak et al.*, 1980]. The origin of the strong absorption in the visible and near-IR is apparently an open issue. *Schlegel et al.* [1979] attribute the absorption to iron $3d^n \rightarrow 3d^{n-1}4s$ orbital promotion processes including final-state effects of the atomlike $3d^{n-1}$ configuration. Others [e.g., *Huguenin*, 1973; *Burns et al.*, 1980] attribute it to intervalence charge-transfer transitions among the ferrous and ferric ions on the octahedral sites. The intense oxide $\rightarrow$ iron-ion charge-transfer transitions can account for the strong absorption in the near-UV as discussed previously for hematite.

Although the above discussion dealt with experiments performed on magnetite, the interpretations are probably applicable at least approximately to the spectra of cation-deficient magnetites because of the similarity in crystal structure, distribution of cations among crystallographic sites, and the Mössbauer studies cited above. The weak reflectivity maximum around 0.80 μm in our spectra (Figure 14) suggests a reflectivity "window" between absorption bands centered in the near-UV and visible and the near-IR, but it could be instead due to a very strong absorption band since such bands in diffuse reflectivity spectra can be positive features [*Vincent and Hunt*, 1968]. The latter is probably not the case here, however, because the data of *Schlegel et al.* [1979] indicate a local minimum in the absorption coefficient near 0.8 μm (their

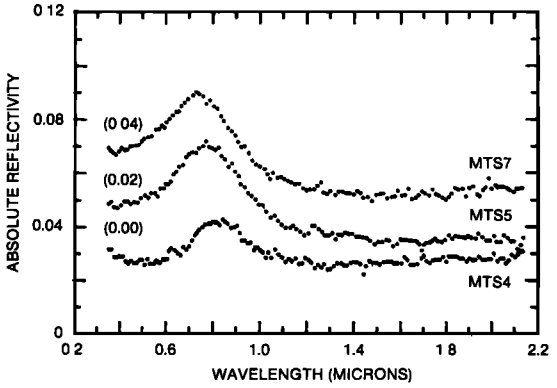

Fig. 14. Diffuse reflectivity spectra of cation-deficient magnetite powders at room temperature.

data are quite compressed in this spectral region). The spectra in Figure 14 also show the reflectivity maximum is more pronounced in the two powders (MTS5 and MTS7) having the most extreme cation deficiency, i.e., lowest FeO content. This correlation between the magnitudes of the reflectivity maximum and the cation deficiency has also been noted by *Sherman et al.* [1982].

Effect of particle size and shape. The limited sample set together with variable composition (i.e., variable degrees of cation deficiency) makes difficult any conclusions regarding the effects of particle size and shape. Magnetite, whose absorption coefficient in our spectral region ranges from about 70,000 to 650,000 cm^{-1} [*Schlegel et al.*, 1979], is a strong absorber, and consequently we would expect its powders to become less reflective with decreasing particle size. This is the case longward of the positive reflectance feature centered around 0.80 μm for the MTS5 and MTS7 powders as compared to the significantly coarser MTS4 powder. The magnitude of the reflectivity at the maximum is slightly higher for the MTS5 and MTS7 powders (about 0.05 as compared to about 0.04 for MTS4), and this may be due to an overriding compositional effect since they are more cation deficient than MTS4 (about 19% as compared to about 23%).

6.3. *Optical Properties: Low Temperature*

The normalized reflectivity spectra of the cation-deficient magnetite powders MTS4 and MTS5 at +20° and about −110°C are shown in Figure 13. Within experimental error, the spectra are independent of temperature over the range between 20° and −110°C. Thus, these cation-deficient magnetites behave similarly to stoichiometric magnetite which, at about −150°C, is still a strong absorber [*Schlegel et al.*, 1979].

7. GOETHITE AND LEPIDOCROCITE POWDERS

7.1. *Material Properties*

The chemical and physical properties of the commercially prepared goethite (α-FeOOH) and lepidocrocite (γ-FeOOH) powders are given in Table 9. Some of these data were reported in an earlier study [*Morris and Lauer*, 1981]. All of these powders have acicular-shaped particles and were prepared by precipitation techniques. As we found for the other powders, the FeOOH powders are nearly pure chemically with SiO_2 and SO_3 being the major impurities. The X ray powder diffraction patterns for the FeOOH powders are consistent with single phase materials [*JCPDS*, 1980], and the sharpness of the diffraction lines (0.20°–0.42° 2θ half width for the four most intense lines) indicate a high degree of crystallinity. As shown by the thermogravimetric data of *Morris and Lauer* [1981], GTS2 and GTS3 dehydrate to hematite by 250°–275°C at a heating rate of ~0.5°C/min. Similarly, LPS2 dehydrates to a strongly magnetic phase (a poorly crystallized maghemite) by ~240°C. We found that under the same experimental conditions GTS5 behaved analogously to GTS2 and GTS3.

TABLE 9. Summary of Selected Physical and Chemical Properties of Commercial Goethite (α-FeOOH) and Lepidocrocite (γ-FeOOH) Powders

	α-FeOOH			γ-FeOOH,
Property*	GTS2	GTS3	GTS5	LPS2
Shape	acic.	acic.	acic.	acic.
M_z	0.05 × 0.4	0.10 × 0.7	0.10 × 0.5	0.03 × 0.9
Range	0.03 × 0.3–0.08 × 0.6	0.05 × 0.4–0.2 × 1.0	0.06 × 0.3–0.2 × 0.8	0.02 × 0.5–0.05 × 1.3
J_s	0.06(2)	0.06(4)	0.10(4)	0.31(6)
IS	0.37(1)	0.37(1)	0.37(1)	0.37(1)
QS	−0.27(1)	−0.27(1)	−0.27(1)	0.53(1)
H_{int}	380(2)	381(2)	381(2)	...
SiO_2	1.04	0.36	1.55	0.84
TiO_2	0.02	0.02	0.00	0.01
Al_2O_3	0.55	0.19	0.00	0.23
Fe_2O_3	83.26	84.20	84.60	84.55
FeO	0.28	0.22	0.32	0.33
MnO	0.13	0.13	0.02	0.17
MgO	0.30	0.21	0.27	0.24
CaO	0.10	0.02	0.15	0.05
K_2O	0.00	0.03	0.00	0.01
P_2O_5	0.00	0.00	0.03	0.03
SO_3	0.84	0.63	0.80	0.07
CO_2	0.29	0.24	0.11	0.21
(+)H_2O	10.02	9.74	10.22	9.84
(−)H_2O	0.58	0.20	0.37	1.08
Total	97.441	96.19	98.44	97.66

Errors are given in parenthesis and refer to the final digit.
*See Table 1.

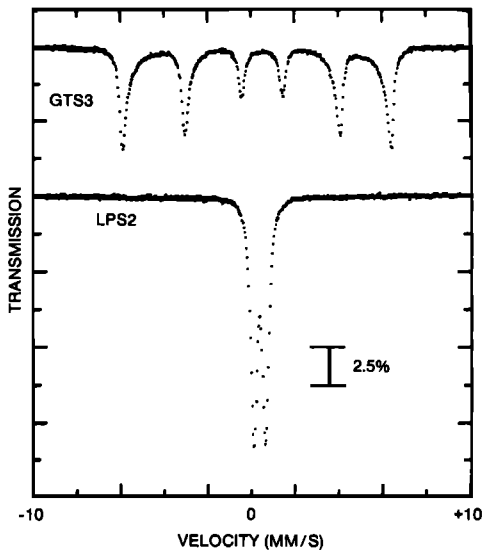

Fig. 15. Mössbauer spectra for goethite powder GTS3 and lepidocrocite powder LPS2 at room temperature.

The values of J_s for the goethite powders are nearly equal to zero, and this is expected for goethite which is antiferromagnetic at room temperature [e.g., *Nagata*, 1961; *Strangway*, 1970]. Lepidocrocite is paramagnetic at room temperature and, consequently, should have a value of J_s equal to zero. The small value actually observed can be accounted for by a maghemite impurity present at ~0.4 wt % (using $J_s = 74$ emu/g for pure maghemite). It may also indicate the near-surface volume of the particles are depleted in H_2O and have become maghemitelike in character. This situation, if present, would be analogous to that for the magnetite powders in the sense that the deficiency is possible because goethite and presumably also lepidocrocite are thermodynamically unstable with respect to dehydration under ambient conditions [e.g., *Gooding*, 1978]. However, the chemical data do not indicate any of the FeOOH powders are detectably deficient in $(+)H_2O$. We cannot use thermomagnetic data to test for maghemite in LPS2 because it dehydrates to a maghemite phase upon heating [*Morris and Lauer*, 1981].

The Mössbauer spectra of all the goethite powders have the expected six-line Zeeman pattern as shown in Figure 15 for GTS3. The values for the isomer shift (0.37 mm/s), quadrupole splitting (−0.27 mm/s), and internal field strength (381 kOe) are in good agreement with the results of *Forsyth et al.* [1968] and *Fysh and Clark* [1982]. As is typical of Mössbauer spectra of goethite at room temperature, the individual Mössbauer lines are asymmetrically broadened toward zero velocity due to the relatively close proximity of the Néel temperature (~127°C) for goethite [*Forsyth et al.*, 1968; *Murad*, 1982]. For the lepidocrocite powder, a quadrupole doublet was observed (Figure 15) having an isomer shift of 0.37 mm/s and a quadrupole splitting of 0.53 mm/s. This is characteristic of lepidocrocite since it is not magnetically ordered at room temperature [*Johnson*, 1969]. Our value for the quadrupole splitting is in good agreement with the result of *Johnson* [1969], but the isomer shift is significantly larger than his 0.30 mm/s value.

In summary, the goethite and lepidocrocite powders are predominantly single-phase materials by the criteria of the above data.

7.2. *Optical Properties: Room Temperature*

Spectra and band assignments. The diffuse reflectivity spectra for the goethite powders GTS2, GTS3, and GTS5 and the lepidocrocite powder LPS2 are given in Figure 16. The spectra of both polymorphs have the same general form. The reflectivity is relatively high longward of the band whose minimum is about 0.90–0.93 μm for the goethite powders and about 0.98 μm for the lepidocrocite powder. Two other bands are discernable at shorter wavelengths. The minimum of one of them is well defined and is near 0.65 μm for the goethites and near 0.70 μm for the lepidocrocite. The minimum of the other band is not well-defined but appears to be around 0.45 μm for both polymorphs. The wings of the three bands define two local reflectivity maxima near 0.76 and 0.59 μm for the goethites and near 0.82 and 0.62 μm for the lepidocrocite. The absorption edge (i.e., the long wavelength edge of the stopping band) occurs in the region 0.38–0.43 μm for both compositions. The measured positions of the above features for each powder are compiled in Table 10. Note that the positions of the features in the lepidocrocite spectrum are at longer wavelengths than the corresponding ones in the goethite spectra.

In contrast with the spectra of the hematite and maghemite powders, we did not find in the FeOOH spectra a knee located longward of the band minimum occurring in the range 0.90–0.98 μm. Since that band in the FeOOH spectra is asymmetric about its minimum and broader than the corresponding one in the Fe_2O_3 spectra, we consider that the band responsible for the knee in the Fe_2O_3 spectra is just relatively more intense in the FeOOH spectra so that its expression is broadening and shape distortion rather than a knee.

Both goethite and lepidocrocite have an orthorhombic crystal structure where the ferric ions are all octahedrally coordinated to oxide ions [e.g., *Murray*, 1979]. They differ, however, in the arrangement of their oxygen atoms [e.g., *Murray*, 1979]; the structure of goethite is based on a hexagonally close-packed lattice, and that of lepidocrocite, a cubic close-packed lattice. As shown in Table 4, the ^4G spectroscopic state is split into nine states by a crystal field having orthorhombic symmetry so that there are a total of nine bands possible from transitions from the $^6A_1$ ground state to the nine ^4G levels.

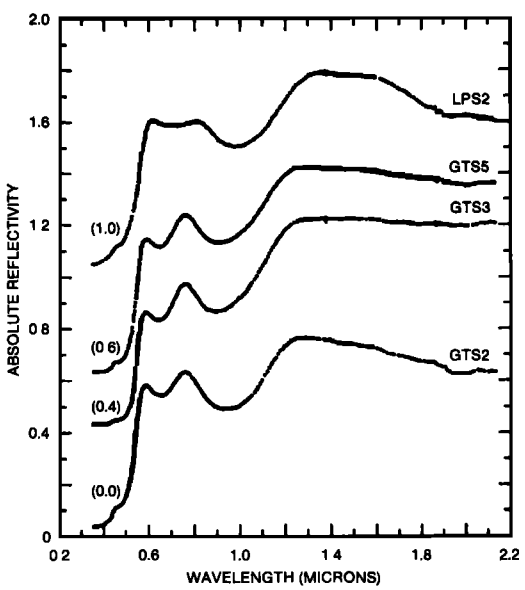

Fig. 16. Diffuse reflectivity spectra for goethite and lepidocrocite powders at room temperature.

TABLE 10. Location of Spectral Features in Goethite and Lepidocrocite Spectra at 25°C

FeOOH	Absorption Edge[a]	Shoulder[a]	Local Reflectivity Maximum[b]	Band Minimum[a]	Local Reflectivity Maximum[b]	Band Minimum[a]
Goethite						
GTS2	0.381	0.445	0.585	0.652	0.761	0.932
GTS3	0.417	0.447	0.585	0.645	0.759	0.896
GTS5	0.429	0.444	0.593	0.648	0.763	0.908
Lepidocrocite						
LPS2	0.393	0.463	0.621	0.704	0.822	0.982

All wavelengths in microns.
[a]Error = ±0.010.
[b]Error = ±0.005.

Unfortunately, there do not seem to be energy level diagrams available in the literature for the more complicated case of orthorhombic symmetry. The procedure usually adopted [e.g., *Hunt and Ashley*, 1979; *Strens and Wood*, 1979; *Singer*, 1982; *Sherman et al.*, 1982] for band assignment for goethite and lepidocrocite is to use the cubic energy level diagram and assign the bands near 0.90, 0.63, and 0.45 μm for goethite and the ones near 0.98, 0.70, and 0.45 μm for lepidocrocite to transitions from $^6A_1$ to the cubic $^4T_1$, $^4T_2$, and (^4E, $^4A_1$) levels, respectively. They are reasonable assignment schemes in that they both have the $^6A_1 \rightarrow (^4E, ^4A_1)$ transition occurring near 0.45 μm. For both polymorphs, we attribute the asymmetric shape of the $^4T_1$ band, which is even more evident in the low-temperature spectra discussed later, to the presence of unresolved bands arising from the splitting of the cubic $^4T_1$ level by a noncubic crystal field. As in the cases of the Fe_2O_3 powders, the region of strong absorption shortward of the absorption edge in the vicinity of 0.38–0.43 μm is attributed to intense oxide → ferric charge-transfer transitions.

It is possible to have bands in the near-IR that are due to overtones and combination tones of the stretching and bending vibrations associated with the OH groups which are present in the crystal structures of goethite and lepidocrocite, as can be shown by calculation using the fundamental vibration frequencies compiled by *Ryskin* [1974]. For goethite, the stretching and two bending fundamental vibrations occur at 3095 cm^{-1} (3.23 μm), 890 cm^{-1} (11.2 μm) and 797 cm^{-1} (12.5 μm), respectively. For lepidocrocite, the stretching fundamental is apparently doubled at 3390 and 3125 cm^{-1} (2.95 and 3.20 μm), and so is one of the bending fundamentals at 1161 and 1026 cm^{-1} (8.6 and 9.7 μm); the other bending fundamental occurs at 753 cm^{-1} (13.3 μm). Thus, the first overtone of the fundamental stretching vibration would be expected near 1.62 μm for goethite and near 1.47 and 1.60 μm for lepidocrocite assuming no significant anharmonicity. It is the first overtone of the stretching vibration of the OH group that gives rise to the strong band near 1.4 μm in a wide variety of other materials that contain OH groups as discrete OH or as H_2O [e.g., *Hunt and Salisbury*, 1970; *Hunt et al.*, 1971].

As can be seen in Figure 16, the spectra of the goethite powders in the near-IR do not contain any strong bands in addition to those previously attributed to ferric iron. There is, for example, no indication of a band near 1.6 μm for the first overtone of the OH stretching vibration. There does appear to be a weak band near 1.95 μm for GTS2 and GTS5, but it could be due to adsorbed atmospheric H_2O. For the lepidocrocite powder there does appear to be a complex structure of overlapping bands whose short wavelength edge is about 1.6 μm and whose long wavelength edge is beyond the wavelength limit of our data (~2.2 μm). Without additional data, we feel this structure is best explained as a composite of bands due to adsorbed atmospheric H_2O and bands due to the OH groups in the structural sites of lepidocrocite.

Effect of particle size and shape. Because of limited data, we can discuss only the goethite powders. As expected, because it has a smaller D_s, GTS5 is more reflective than GTS3 except shortward of the absorption edge where the reflectivities are comparable. However, that situation may be fortuitous because their mean particle sizes overlap at the one standard deviation level. Because the value of D_s for GTS2 is about half those for GTS3 and GTS5, we expected it to be the most reflective of the three goethite powders. It does have the highest reflectivity between the local reflectivity maximum near 0.59 μm and the absorption edge. For wavelengths longer than ~0.55 μm it is less reflective than GTS3; for GTS5, the crossover point is about 1.2 μm. Data on additional powders covering a wider range of mean particle diameters are required to extend this discussion further.

The positions of the two band minima of the goethite powders increase with decreasing mean particle diameter; for example, the band minimum at ~0.93 μm for GTS2 is ~0.03 μm longward of the minimum at ~0.90 μm for GTS3. We observed similar behavior for the band minimum in the spectra of the hematite powders (see Figure 7) and suggested there that the observed dependence might be due to wavelength-dependent scattering. It follows that, since lepidocrocite LPS2 has about the same value of D_s as GTS2, the band positions for coarser-grained equivalents of LPS2 probably are at somewhat shorter wavelengths.

7.3. *Optical Properties: Low Temperature*

The normalized reflectivity spectra for GTS2, GTS3 and LPS2 at about +20° and −110°C are shown in Figure 17; GTS5 behaved similarly to GTS3. As we found for the spectra of the ferric oxide powders, reduced temperatures resulted in an apparent reduction in the width of the bands which contribute to the spectra resulting in the observed general steepening of slopes and the small increase in optical contrast between the band minima and the local reflectivity maxima. For the goethites, the band minimum near 0.93 μm for GTS2 and 0.90 μm for GTS3 and the two local reflectivity maxima for both powders shift shortward by about 0.02–0.03 μm by −110°C; spectra obtained at intermediate temperatures show this shift is a smooth function of temperature. The positions of the other spectral features at about −110°C are within 0.01 μm of the values at 20°C tabulated in Table 10. For lepidocrocite LPS2, the band minimum near 0.98 μm and the local reflectivity maximum near 0.59 μm at 20°C shift shortward by about 0.02–0.03 μm by −110°C. The local reflectivity maximum near 0.82 μm at 20°C, however, shifts longward by about

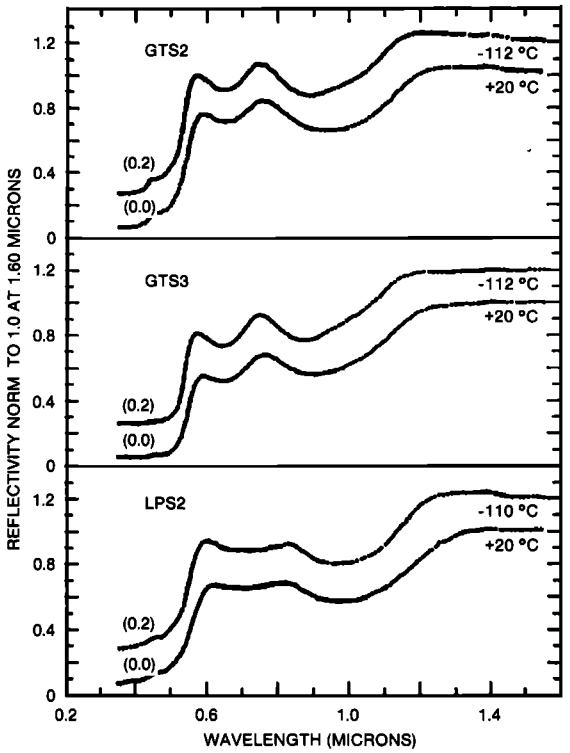

Fig. 17. Normalized reflectivity spectra for goethite powders GTS2 and GTS3 and lepidocrocite powder LPS2 at about +20° and −110°C. See caption of Figure 9.

0.02 μm. The band minimum near 0.70 μm at 20°C does not appear to change position to within 0.01 μm at low temperature.

Sherman et al. [1982] reported that the minimum of the $^4T_1$ feature shifted 0.03 μm to shorter wavelengths at −10°C relative to its position at room temperature. Although the direction of the shift is the same, we did not observe a shift of this magnitude until about −110°C, and the shape of the feature is also somewhat different. The shift we observed at about −10°C was less than 0.01 μm. The origin of this difference may be due to different samples, but there is no direct evidence for this.

8. Systematics in Band Positions

Energy level diagrams including those in Figure 4 for a d^5 ion like ferric iron show that the energies at which crystal field levels occur are a complex function of many parameters. The Racah B and C parameters are a measure of interelectron repulsion and bond covalency. The number of crystal field parameters is determined by symmetry considerations, and their magnitudes depend on such factors as the type of ligand, coordination number, and the length of the metal-ligand bond. We discuss below whether the observed range in the position of corresponding spectral bands among the ferric oxides and oxyhydroxides can be reasonably attributed to a single effect. We will consider only the band assigned to the envelope of the transitions from $^6A_1$ to the split components of the cubic $^4T_1$ level for octahedrally-coordinated iron since that band is the only one well defined in all of our ferric-compound spectra. In Table 11 are listed the ferric oxides and oxyhydroxides in order of increasing wavelength for the position of the band minimum together with literature data for the ferric-oxide bond lengths and the internal field strength (H_{int}) at low temperature determined by Mössbauer spectroscopy.

TABLE 11. Band Minima for the Envelope of the Split Components of the Cubic $^4T_1$ Band (This Study), Average and Minimum Octahedral Fe-O Bond Lengths [*Wycoff*, 1963; *Blake et al.*, 1966; *Prevot and Poix*, 1971] and H_{int} at 4.2°K [*Forsyth et al.*, 1968; *Johnson*, 1969] for Ferric Oxides and Oxyhydroxides

Compound	Band Minimum, μm	Fe-O, A		H_{int}, kOe, at 4.2°K
		Average	Minimum	
α-Fe_2O_3	0.85–0.87	2.03	1.945	540
α-FeOOH	0.90–0.93	2.03	1.87	504
γ-Fe_2O_3	0.92–0.94	2.03	···	515*
γ-FeOOH	0.98	2.04	1.94	460

*Calculated assuming temperature dependence of the Brillouin function.

In the electrostatic representation of the cubic crystal-field potential, the dependence of the cubic crystal field parameter Dq on the metal-ligand bond length R is given adequately by $Dq \propto R^{-5}$ [e.g., *Low*, 1960]. Thus, even small differences in R can give rise to significant differences in Dq and thus in the positions of the crystal-field bands. With respect to the energy level diagrams for ferric iron (Figure 4), a shift to longer wavelengths in the position of the band minimum would result from a contraction of the ferric-oxide bond with all other parameters held constant. The data in Table 11 show that the bond length is essentially constant. Thus the observed range in the position of the band minimum does not appear to be due to variable ferric-oxide bond lengths.

The magnitude of H_{int} for compounds of ferric iron is considered to be a good measure of the extent of bond covalency with more covalent compounds having relatively lower values of H_{int} [e.g., *Greenwood and Gibb*, 1971]. As can be seen in the energy level diagrams (Figure 4), increased covalent character shifts the band minimum to longer wavelengths because the values of the Racah B and C parameters are reduced [e.g., *Marfunin*, 1979]. Therefore, if all factors (except the degree of bond covalency) which affect the band-minimum wavelength and the value of H_{int} are sufficiently constant for a series of ferric compounds, we would expect a negative correlation between the band-minimum wavelength and H_{int}. When the oxides and oxyhydroxides (see Table 11) are considered separately, the position of the band minimum is at a longer wavelength for the compound having the smaller H_{int}. If all four ferric compounds are considered in order of increasing values of the band minimum in wavelength units, the values of H_{int} for γ-Fe_2O_3 and α-FeOOH are out of order. This may not be significant since the ranges for their band minima overlap and the value of H_{int} for γ-Fe_2O_3 was estimated. However, it may be that other factors, such as shifts in the minimum of the $^4T_1$ level in noncubic environments, are not sufficiently constant and thus obscure to some extent the relationship between the envelope minimum and H_{int}. Nevertheless, the range observed for the band minima among the ferric compounds appears to be related at least in part to differences in the degree of covalency of the ferric-oxygen bond.

9. Application to Remote Sensing of Planetary Surfaces

An inverse problem of the spectral properties of well-characterized laboratory samples is to infer physicochemical properties of planetary surfaces from their spectral signatures, which are derived mainly from earth-based telescopic observations and spacecraft imagery. It is difficult to establish unique-

ness in such inversions because variations in different physicochemical properties can have the same effect on reflectance spectra and, more fundamentally, because many of the optically important physicochemical parameters have not been investigated in a systematic way in laboratory and theoretical studies. This study directly addresses the latter consideration with respect to the earth and Mars where iron oxides and oxyhydroxides are optically important. We will briefly discuss the applications of the results of this study to the remote sensing of those bodies but will not in this paper use these and other data to discuss interpretations inferred from planetary reflectance spectra.

An important part of the spectral data base for Mars with respect to ferric oxides and oxyhydroxides is the Viking orbiter multispectral images obtained with bandpass filters centered near 0.45, 0.53 and 0.59 μm. Recently, *McCord et al.* [1982] have used these data to define units of similar optical properties for a large part of the martian surface on a variation diagram of the red (0.59 μm) and violet (0.45 μm) albedo values. Included on this diagram are single data points for hematite and goethite, and they do not fall within the range of the martian data. One of the results of this study is that a range of values rather than a single value is characteristic of hematite just due to variations in the mean particle diameter between about 0.10 and 1.0 μm. The ranges we observed were about 0.03–0.04 at 0.45 μm and about 0.06–0.30 at 0.59 μm. Even allowing for some difference because we did not convolve our data to the bandpass of the Viking filters, this range partially overlaps the martian data and also includes the hematite datum of *McCord et al.* [1982]. Our corresponding data for goethite includes the goethite datum of *McCord et al.* [1982], but both do not overlap the martian data. Based on our experience with the hematite powders, this might not be the case if our goethite powders had spanned a larger range in mean particle diameter. Our data for maghemite, a phase not considered by *McCord et al.* [1982] but inferred to be present on the basis of the Viking magnetic properties experiment [*Hargraves et al.*, 1979], fall just outside the envelope of the martian data. For the three maghemite powders, the ranges in reflectivity are about 0.035–0.040 at 0.45 μm and about 0.17–0.23 at 0.59 μm. Presumably, corresponding data for coarser maghemite powders would also fall within the envelope of the martian data.

A potential complication to the preceding discussion is that the target materials are not at the same temperature. The data for the laboratory samples were obtained at room temperature. For the surface of Mars, the temperature range measured by the Viking landers was between about −120 and −20°C [*Ryan and Henry*, 1979]. Our low temperature measurements showed that, although the positions of spectral bands were relatively insensitive to temperature, a general steepening of slopes occurred with decreasing temperature. Thus, measurements on slopes, such as at 0.59 μm for the iron oxides, will depend somewhat on temperature.

It is important to recognize that the spectral properties of the iron oxides and oxyhydroxides powders were determined relative to an air (or N_2) matrix which has an index of refraction nearly equal to 1.0. On Mars these phases, if present in finely divided form, are more likely to occur imbedded in solid H_2O/CO_2 or silicate matrices which have indices of refraction significantly greater than 1.0. Since the magnitude of reflectivity is strongly dependent on the contrast in the index of refraction between the iron oxides and oxyhydroxides and that of the surrounding matrix [e.g., *Hottel et al.*, 1968; *Kortum*, 1969], inferences as to the presence or absence of these phases on Mars on the basis of correlation diagrams like that of *McCord et al.* [1982] are not unambiguous.

Remote sensing of the earth has economic importance as a tool in mapping ore deposits. This is a very complex problem, but it, in part, involves mapping iron oxides and oxyhydroxides which are, but not uniquely, produced during weathering of iron sulfides associated with hydrothermal mineralization. *Buckingham and Sommer* [1983] have argued that these iron oxides and oxyhydroxides are depleted in aluminum relative to their counterparts formed during weathering of silicate material and that this difference might be detectable remotely since aluminum substitution alters the spectral properties. For the reflectivity minimum in the near-IR, they report a shift of about 0.02 μm to longer wavelengths for goethite having about 33% aluminum. We found that comparable shifts can also be produced by particle-size effects so that spectral variation due to this cause should also be considered.

10. Summary and Conclusions

1. A variety of physical and chemical data are necessary to establish the actual nature of nominal hematite, maghemite, magnetite, goethite, and lepidocrocite submicron powders and to interpret their reflectance spectra. Some of the nominal hematite powders contain optically significant amounts of magnetite or cation-deficient magnetite that strongly influenced their spectral properties in the near-IR. All of the nominal magnetite powders are actually cation-deficient magnetites having down to about 18.0 wt % FeO as compared to about 31.0 wt % for stoichiometric magnetite.

2. A structured absorption edge extending from weak absorption in the near-IR to very strong absorption in the near-UV is characteristic of the ferric oxides and oxyhydroxides and responsible for their intense color. The structure is due to ferric crystal-field bands, and they, as opposed to the tail of the oxide → ferric charge-transfer bands centered in the UV, probably account for most of the absorption in the edge.

3. The position of the crystal-field band at lowest energy is near 0.86, 0.91, 0.92, and 0.98 μm at room temperature for hematite, goethite, maghemite, and lepidocrocite, respectively. Comparison with Mössbauer data suggests the variability is due, at least in part, to differences in bond covalency with increasing wavelength of the minimum indicating increased covalent character.

4. For hematite in particular, the cubic energy level diagram is not a completely adequate representation for assignment of the crystal-field bands. The number and position of the spectral features are consistent with significant splitting of some of the degenerate cubic levels by significant noncubic components of the crystal field. The band discussed in the last paragraph is interpreted as the envelope of bands due to the split cubic $^4T_1$ level.

5. The positions of the spectral features for the hematite and maghemite powders are independent of temperature to within about 0.01 μm over the interval between about +20° and −110°C. For the goethite and lepidocrocite powders, a small shift of about 0.02 μm to shorter wavelengths is observed for some of the features after cooling to about −110°C. The main effect of low temperature is to sharpen the spectral features.

6. A detailed examination of the effect of mean particle diameter on spectral properties was possible only for the hematite powders where there was a sufficient number of powders over a sufficiently wide range of mean particle diameters.

Variations in the magnitude of the reflectivity are consistent with scattering theory and depend on the absorption strength in the wavelength interval of interest. The absorption strength of the crystal-field bands increases with increasing mean particle diameter over the range 0.1–0.8 μm. Visually, this corresponds to a color change from orange to deep purple. The position of the envelope of the split $^4T_1$ cubic level shifts to longer wavelengths from about 0.85 to 0.87 μm with decreasing mean particle diameter from 0.8 to 0.1 μm. This effect is consistent with wavelength dependent scattering.

7. The cation-deficient magnetite powders are very strong absorbers throughout the near-UV, visible, and near-IR having at most a maximum reflectivity of about 0.05. Their reflectance spectra are independent of temperature over the range between about +20° and −110°C.

8. The dependence of the spectral properties of the fine powders of iron oxides and oxyhydroxides have applications to the interpretation of remote-sensing spectra of the earth and Mars where those compounds are optically important.

Acknowledgments. This paper benefited from the comments of J. Gooding, W. Mendell, R. Burns, and R. Huguenin. We thank M. D. Dyar for supplying the program DSTONE for reduction of the Mössbauer spectra. We thank E. Stockton and D. Garrick for typing the manuscript.

REFERENCES

Armstrong, R. J., A. H. Morrish, and G. A. Sawatzky, Mössbauer study of ferric ions in a spinel, *Phys. Lett., 23*, 414–416, 1966.

Blake, R. L., R. E. Hessevick, T. Zoltai, and L. W. Finger, Refinement of the hematite structure, *Am. Mineral., 51*, 123–129, 1966.

Bernal, J. D., D. R. Dasgupta, and A. L. MacKay, The oxides and hydroxides of iron and their structural inter-relationships, *Clay Min. Bull., 4*, 15–30, 1959.

Bozorth, R. M., *Ferromagnetism*, D. Van Nostrand, Princeton, N. J., 1951.

Buckingham, W. F., and S. E. Sommer, Mineralogical characterization of rock surfaces formed by hydrothermal alteration and weathering—Application to remote sensing, *Econ. Geol., 78*, 664–674, 1983.

Burns, R. G., D. A. Nolet, K. M. Parkin, C. A. McCammon, and K. B. Schwartz, Mixed-valence minerals of iron and titanium: Correlations of structural, Mössbauer, and electronic spectral data, in *Mixed-Valence Compounds*, edited by D. B. Brown, pp. 295–336, D. Reidel, Hingham, Mass., 1980.

Chen, C. T., and B. D. Cahan, Visible and ultraviolet optical properties of single-crystal and polycrystalline hematite measured by spectroscopic ellipsometry, *J. Opt. Soc. Am., 71*, 932–934, 1981.

Cotton, F. A., *Chemical Applications of Group Theory*, Interscience, New York, 1963.

Daniels, J. M., and A. Rosencwaig, Mössbauer spectroscopy of stoichiometric and non-stoichiometric magnetite, *J. Phys. Chem. Solids, 30*, 1561–1571, 1969.

DeGrave, E., L. H. Bowen, and S. B. Weed, Mössbauer study of aluminum-substituted hematites, *J. Magn. Magn. Mater., 27*, 98–108, 1982.

Dunlop, D. J., Superparamagnetic and single-domain threshold sizes in magnetite, *J. Geophys. Res., 78*, 1780–1793, 1973.

Folk, R. L., and V. C. Ward, Brazos River Bar, a study in the significance of grain-size parameters, *J. Sediment. Petrol., 27*, 3–26, 1957.

Forsyth, J. B., I. O. Hedley, and C. E. Johnson, The magnetic structure and hyperfine field of goethite (α-FeOOH), *J. Phys. C, 1*, 179–188, 1968.

Fysh, S. A., and P. E. Clark, Aluminous goethite: A Mössbauer study, *Phys. Chem. Miner., 8*, 180–187, 1982.

Gibson, E. K., Jr., and G. W. Moore, Carbon and sulfur distributions and abundances in lunar fines, *Proc. Lunar Sci. Conf., 4th*, 1577–1586, 1973.

Goodenough, J. B., The Verwey transition revisited, in *Mixed-Valence Compounds*, edited by D. B. Brown, pp. 413–425, D. Reidel, Hingham, Mass., 1980.

Gooding, J. L., Chemical weathering on Mars: Thermodynamic stabilities of primary minerals (and their alteration products) from mafic igneous rocks, *Icarus, 33*, 483–513, 1978.

Greenwood, N. N., and T. C. Gibb, *Mössbauer Spectroscopy*, Chapman and Hall, London, 1971.

Hancock, K. R., Mineral pigments, in *Industrial Minerals and Rocks*, 4th ed., pp. 335–357, American Institute of Mining, Metallurgical, and Petroleum Engineers, Baltimore, Md., 1975.

Hargraves, R. B., D. W. Collinson, R. E. Arvidson, and P. M. Cates, Viking magnetic properties experiment: Extended mission results, *J. Geophys. Res., 84*, 8379–8384, 1979.

Hedelman, S., and W. N. Mitchell, Some new diffuse and specular reflectance accessories for the Cary Models 14 and 15 spectrophotometer, in *Modern Aspects of Reflectance Spectroscopy*, edited by W. W. Wendlandt, pp. 158–169, Plenum, New York, 1968.

Hottel, H. C., A. F. Sarofim, L. B. Evans, and I. A. Vasalos, Radiative transfer in anisotropically scattering media: Allowance for fresnel reflection at the boundaries, *J. Heat Transfer, C90*, 56–62, 1968.

Huguenin, R. L., Photostimulated oxidation of magnetite, 1, Kinetics and alteration phase identification, *J. Geophys. Res., 78*, 8481–8493, 1973.

Huguenin, R. L., Mars: Surface mineralogy from reflectance spectra (abstract), *Lunar Planet. Sci., 8*, 478–480, 1977.

Hunt, G. R., and R. P. Ashley, Spectra of altered rocks in the visible and near infrared, *Econ. Geol., 74*, 1613–1629, 1979.

Hunt, G. R., and J. W. Salisbury, Visible and near-infrared spectra of minerals and rocks, I, Silicate minerals, *Mod. Geol., 1*, 283–300, 1970.

Hunt, G. R., J. W. Salisbury, and C. J. Lenhoff, Visible and near-infrared spectra of minerals and rocks, III, Oxides and hydroxides, *Mod. Geol., 2*, 195–205, 1971.

Joint Committee on Powder Diffraction Standards (JCPDS), *Mineral Powder Diffraction File: Data Book*, JCPDS International Center for Diffraction Data, Swarthmore, Pa., 1980.

Johnson, C. E., Antiferromagnetism of FeOOH: A Mössbauer effect study, *J. Phys. C, 2*, 1996–2002, 1969.

Johnson, H. P., and R. T. Merrill, Low-temperature oxidation of a single-domain magnetite, *J. Geophys. Res., 79*, 5533–5534, 1974.

Kahn, F. J., P. S. Pershan, and J. P. Remeika, Ultraviolet magneto-optical properties of single-crystal orthoferrites, garnets, and other ferric oxide compounds, *Phys. Rev., 186*, 891–918, 1969.

Konig, E., and S. Kremer, *Ligand Field Energy Diagrams*, Plenum, New York, 1977.

Kortum, G., *Reflectance Spectroscopy*, Springer-Verlag, New York, 1969.

Krebs, J. J., and W. G. Maisch, Exchange effects in the optical-absorption of Fe^{3+} in Al_2O_3, *Phys. Rev. B, 4*, 757–769, 1971.

Lehmann, G., and H. Harder, Optical spectra of di- and trivalent iron in corundum, *Am. Mineral., 5*, 98–105, 1970.

Lindsley, D. H., The crystal chemistry and structure of oxide minerals as exemplified by the Fe-Ti oxides, Oxide Minerals, *Short Course Notes Mineral. Soc. Am., 3*, L-1–L-60, 1976.

Low, W., *Paramagnetic Resonance in Solids*, suppl. 2, *Solid State Physics*, Academic, Orlando, Fla., 1960.

Marfunin, A. S., *Physics of Minerals and Inorganic Materials*, Springer-Verlag, New York, 1979.

Marusak, L. A., R. Messier, and W. B. White, Optical absorption spectrum of hematite, Fe_2O_3 near IR to UV, *J. Phys. Chem. Solids, 41*, 981–984, 1980.

Maxwell, J. A., *Rock and Mineral Analysis*, pp. 419–421, Interscience, New York, 1968.

McCord, T. B., R. B. Singer, B. R. Hawke, J. B. Adams, D. L. Evans, J. W. Head, P. J. Mouginis-Mark, C. M. Pieters, R. L. Huguenin, and S. H. Zisk, Mars: Definition and characterization of global surface units with emphasis on composition, *J. Geophys. Res., 87*, 10,129–10,148, 1982.

Morris, R. V., and H. V. Lauer, Jr., The case against UV photostimulated oxidation of magnetite, *Geophys. Res. Lett., 7*, 605–608, 1980.

Morris, R. V., and H. V. Lauer, Jr., Stability of goethite (α-FeOOH) and lipidocrocite (γ-FeOOH) to dehydration by UV radiation: Implication for their occurrence on the martian surface, *J. Geophys. Res., 86*, 10,893–10,899, 1981.

Morris, R. V., and H. V. Lauer, Jr., Optical spectra and band assignments for the hematite (α-Fe_2O_3)-corundum (α-Al_2O_3) series (abstract), *Lunar Planet. Sci., 14*, 534–525, 1983.

Morris, R. V., and S. C. Neely, Optical properties of hematite-magnetite mixtures: Implications for Mars, *Lunar Planet. Sci.*, 3, 548–549, 1982.

Morris, R. V., S. C. Neely, and W. W. Mendell, Application of the

Kubelka-Munk theory of diffuse reflectance to geologic problems: The role of scattering, *Geophys. Res. Lett.*, *9*, 113–116, 1982.
Murad, E., The characterization of goethite by Mössbauer aspectroscopy, *Am. Mineral.*, *67*, 1007–1011, 1982.
Murray, J. W., Iron oxides, Marine Minerals, *Short Course Notes, Mineral. Soc. Am.*, *6*, 47–98, 1979.
Nagata, T., *Rock Magnetism*, Plenum, New York, 1961.
Norrish, K., and B. W. Chappell, X-ray fluorescence spectrography, in *Physical Methods in Determinative Mineralogy*, edited by J. Zussman, Academic, Orlando, Fla., 1967.
Norrish, K., and J. T. Hutton, An accurate X-ray spectrograph method for the analysis of a wide range of geological samples, *Geochim. Cosmochim. Acat*, *33*, 431–454, 1969.
Prevot, M, and P. Poix, Un calcul du porametre cristallin des titanomagnetites oxydees, *J. Geomagn. Geoelectr.*, *23*, 255–265, 1971.
Ryan, J. A., and R. M. Henry, Mars atmospheric phenomena during major dust storms, as measured at surface, *J. Geophys. Res.*, *84*, 2821–2829, 1979.
Ryskin, Ya. I., The vibrations of protons in minerals: Hydroxyl, water and ammonium, in *The Infrared Spectra of Minerals*, edited by V. C. Farmer, pp. 137–181, Mineralogical Society, London, 1974.
Schlegel, A., S. F. Alvarado, and P. Wachter, Optical properties of magnetite (Fe_3O_4), *J. Phys. C Solid State Phys.*, *12*, 1157–1164, 1979.
Sherman, D. M., R. G. Burns, and V. M. Burns, Spectral characteristics of the iron oxides with application to the martian bright region mineralogy, *J. Geophys. Res.*, *87*, 10,169–10,180, 1982.
Singer, R. B., Spectral evidence for the mineralogy of high-albedo soils and dust on Mars, *J. Geophys. Res.*, *87*, 10,159–10,168, 1982.
Soderblom, L. A., K. Edwards, E. M. Eliason, E. M. Sanchez, and M. P. Charette, Global color variations on the martian surface, *Icarus*, *34*, 446–464, 1978.
Stone, A. J., H. J. Augard, and J. Fenger, MOSSPEC program for resolving Mössbauer spectra, *Risoe Rep. RISO-M-1348*, Danish At. Energy Comm., Roskilde, Den., 1971.
Stoner, E. C., and E. P. Wohlfarth, A mechanism of magnetic hysteresis in heterogeneous alloys, *Philos. Trans. R. Soc. London Ser. A*, *A240*, 599–642, 1948.
Strangway, D. W., *History of the Earth's Magnetic Field*, McGraw-Hill, New York, 1970.
Strens, R. G. J., and B. J. Wood, Diffuse reflectance spectra and optical properties of some iron and titanium oxides and oxyhydroxides, *Mineral. Mag.*, *43*, 347–354, 1979.
Tossell, J. A., D. J. Vaughan, and K. H. Johnson, The electronic structure of ferric iron octahedrally coordinated to oxygen: A fundamental polyhedral unit of iron-bearing oxide and silicate minerals, *Nature*, *244*, 42–45, 1973.
Verwey, E. J. W., and P. W. Haayman, Electronic conductivity and transition point of magnetite, *Physica*, *8*, 979–987, 1941.
Vincent, R. K., and G. R. Hunt, Infrared reflectance from mat surfaces, *Appl. Opt.*, *7*, 53–59, 1968.
Weidner, V. R., and J. J. Hsia, Reflection properties of pressed polytetrafluoroethylene powder, *J. Opt. Soc. Am.*, *71*, 856–861, 1981.
Wendlandt, W. W., and H. G. Hecht, *Reflectance Spectroscopy*, Interscience, New York, 1966.
Wood, D. L., and J. P. Remeika, Effect of impurities on the optical properties of yttrium iron garnet, *J. Appl. Phys.*, *38*, 1038–1045, 1967.
Wycoff, R. G. W., *Crystal Structures*, vol. II, Interscience, New York, 1963.

E. K. Gibson, Jr., R. V. Morris, and C. A. Lawson, NASA Johnson Space Center, SN4-83-L110, Houston, TX 77058.
H. V. Lauer, Jr., G. A. Nace, and C. Stewart, Lockheed, 1830 NASA Road 1, Houston, TX 77058.

(Received October 17, 1983;
revised September 19, 1984;
accepted October 26, 1984.)